

Convergence rate of dimension reduction in Bose-Einstein condensates

Weizhu Bao¹, Yunyi Ge¹, Dieter Jaksch², Peter A. Markowich³ and Rada M. Weishäupl³

¹ Department of Mathematics and Center for Computational Science & Engineering, National University of Singapore, Singapore 117543. Email: *bao@math.nus.edu.sg* (W.B.) and *yunyi.ge@nus.edu.sg* (Y.G.)

²Clarendon Laboratory, Department of Physics, University of Oxford, Oxford, United Kingdom. Email: *Dieter.Jaksch@physics.ox.ac.uk*.

³Institut für Mathematik, Universität Wien, Nordbergstr. 15, 1090 Vienna, Austria. Email: *peter.markowich@univie.ac.at* (P.A.M.) and *rada.weishaeupl@univie.ac.at* (R.M.W.)

Abstract

In this paper, we study dimension reduction of the three-dimensional (3D) Gross-Pitaevskii equation (GPE) modelling Bose-Einstein condensation under different limiting interaction and trapping frequencies parameter regimes. Convergence rates for the dimension reduction of 3D ground state and dynamics of the GPE in the case of disk-shaped condensation and cigar-shaped condensation are reported based on our asymptotic and numerical results. In addition, the parameter regimes in which the 3D GPE cannot be reduced to lower dimensions are identified.

1 Introduction

Since its realization in dilute bosonic atomic gases [1, 16, 11], Bose-Einstein condensation (BEC) has been produced and studied extensively in the laboratory [27, 29, 20], and has afforded an intriguing glimpse into the macroscopic quantum world [29]. The experimental advances in BEC have spurred great excitement in the atomic physics community and renewed the interest in studying the collective dynamics of macroscopic ensembles of atoms occupying the same one-particle quantum state. Needless to say that this dramatic progress on the experimental front has stimulated a wave of activity on both the theoretical and the numerical front.

At temperatures T much smaller than the critical temperature T_c [22], a weakly interacting BEC is well described by the macroscopic wave function $\psi = \psi(\mathbf{x}, t)$

whose evolution is governed by a self-consistent, mean field nonlinear Schrödinger equation (NLSE) known as the Gross-Pitaevskii equation (GPE) [19, 28, 29]

$$i\hbar \frac{\partial \psi(\mathbf{x}, t)}{\partial t} = -\frac{\hbar^2}{2m} \nabla^2 \psi(\mathbf{x}, t) + V(\mathbf{x})\psi(\mathbf{x}, t) + NU_0 |\psi(\mathbf{x}, t)|^2 \psi(\mathbf{x}, t), \quad (1.1)$$

where $\mathbf{x} = (x, y, z)$ is the spatial coordinate, m is the atomic mass, \hbar is the Planck constant, N is the number of particles in the condensate, $V(\mathbf{x})$ is an external trapping potential. When a harmonic trap potential is considered, $V(\mathbf{x}) = \frac{m}{2} (\omega_x^2 x^2 + \omega_y^2 y^2 + \omega_z^2 z^2)$ with ω_x , ω_y and ω_z being the trap frequencies in x , y and z -direction, respectively. Without loss of generality, we assume $\omega_x \leq \omega_y \leq \omega_z$. $U_0 = \frac{4\pi\hbar^2 a_s}{m}$ describes the interaction between atoms in the condensate with a_s the s -wave scattering length. The wave function is normalized according to

$$\int_{\mathbb{R}^3} |\psi(\mathbf{x}, t)|^2 d\mathbf{x} = 1. \quad (1.2)$$

Following the physical literatures [12, 7, 5, 29], introducing the rescaling: $t \rightarrow \frac{t}{\omega_x}$, $\mathbf{x} \rightarrow a_0 \mathbf{x}$ with $a_0 = \sqrt{\frac{\hbar}{m\omega_x}}$, and $\psi \rightarrow \frac{\psi}{a_0^{3/2}}$, we get the following dimensionless GPE under the normalization (1.2) in 3D:

$$i \frac{\partial \psi(\mathbf{x}, t)}{\partial t} = -\frac{1}{2} \nabla^2 \psi(\mathbf{x}, t) + V(\mathbf{x})\psi(\mathbf{x}, t) + \beta |\psi(\mathbf{x}, t)|^2 \psi(\mathbf{x}, t), \quad (1.3)$$

where $\beta = \frac{U_0 N}{a_0^3 \hbar \omega_x} = \frac{4\pi a_s N}{a_0}$ and $V(\mathbf{x}) = \frac{1}{2} (x^2 + \gamma_y^2 y^2 + \gamma_z^2 z^2)$ with $\gamma_y = \frac{\omega_y}{\omega_x}$ and $\gamma_z = \frac{\omega_z}{\omega_x}$.

To find the stationary solution of (1.3), we write

$$\psi(\mathbf{x}, t) = \phi(\mathbf{x}) e^{-i\mu t}, \quad (1.4)$$

where μ is the chemical potential of the condensate and $\phi(\mathbf{x})$ is a function independent of time. Substituting (1.4) into (1.3) gives the following equation for $(\mu, \phi(\mathbf{x}))$:

$$\mu \phi(\mathbf{x}) = -\frac{1}{2} \nabla^2 \phi(\mathbf{x}) + V(\mathbf{x})\phi(\mathbf{x}) + \beta |\phi(\mathbf{x})|^2 \phi(\mathbf{x}), \quad \mathbf{x} \in \mathbb{R}^3, \quad (1.5)$$

under the normalization condition (1.2) with $\psi = \phi$.

This is a nonlinear eigenvalue problem with a constraint and any eigenvalue μ can be computed from its corresponding eigenfunction $\phi(\mathbf{x})$ by

$$\mu = \mu(\phi) = \int_{\mathbb{R}^3} \left[\frac{1}{2} |\nabla \phi(\mathbf{x})|^2 + V(\mathbf{x}) |\phi(\mathbf{x})|^2 + \beta |\phi(\mathbf{x})|^4 \right] d\mathbf{x} = E(\phi) + E_{\text{int}}(\phi), \quad (1.6)$$

where

$$E(\phi) = \int_{\mathbb{R}^3} \left[\frac{1}{2} |\nabla \phi(\mathbf{x})|^2 + V(\mathbf{x}) |\phi(\mathbf{x})|^2 + \frac{\beta}{2} |\phi(\mathbf{x})|^4 \right] d\mathbf{x}, \quad (1.7)$$

$$E_{\text{int}}(\phi) = \frac{\beta}{2} \int_{\mathbb{R}^3} |\phi(\mathbf{x})|^4 d\mathbf{x}, \quad E_{\text{kin}}(\phi) = \int_{\mathbb{R}^3} \frac{1}{2} |\nabla \phi(\mathbf{x})|^2 d\mathbf{x}. \quad (1.8)$$

The ground state of a BEC is usually defined as the minimizer of the following minimization problem:

Find $(\mu_g, \phi_g \in S)$ such that

$$E_g := E(\phi_g) = \min_{\phi \in S} E(\phi), \quad \mu_g := \mu(\phi_g) = E(\phi_g) + E_{\text{int}}(\phi_g), \quad (1.9)$$

where $S = \{\phi \mid \|\phi\| = 1, E(\phi) < \infty\}$ is the unit sphere. The existence of a unique positive minimizer of the minimization problem (1.9) is given in [25].

In an experimental setup, the trapping frequencies in different directions can be very different. Especially, disk-shaped and cigar-shaped condensation were observed in experiments [9, 15, 24, 29]. The 3D GPE (1.3) is formally reduced to 2D GPE in disk-shaped condensation and to 1D GPE in cigar-shaped condensation in the literatures [15, 26, 31, 24, 29, 25, 23, 7, 5, 3, 30]. Mathematical and numerical justification for the dimension reduction of 3D GPE is only available in the weakly interaction regime, i.e. $\beta = o(1)$ [6, 10]. Unfortunately, in the intermediate or strong interaction regime, no results are available. The aim of this paper is to study dimension reduction of the 3D GPE (1.3) under different limiting parameter regimes. In addition, we will provide convergence rate for the dimension reduction based on our asymptotic and numerical results.

The paper is organized as follows. In section 2 we study dimension reduction for the ground state of the 3D GPE (1.5) with repulsive interaction $\beta > 0$ and provide convergence rates. Convergence rate for dimension reduction of 3D time-dependent GPE (1.3) is reported in section 3. Finally some conclusions are drawn in section 4.

2 Dimension reduction for ground states

In this section, we will discuss dimension reduction for BEC ground states and derive approximate ground states as well as their energy and chemical potential for the 3D GPE (1.5) under different parameter regimes of β , γ_y and γ_z .

2.1 Isotropic shaped condensation

In the case of isotropic condensates, i.e. $\gamma_y = O(1)$ and $\gamma_z = O(1)$ ($\iff \omega_y \approx \omega_x$ and $\omega_z \approx \omega_x$), there are three typical regimes:

Regime I. Weakly interacting regime, i.e. $\beta = o(1)$, the ground state is well approximated by the harmonic oscillator ground state [13, 15, 29, 7]:

$$\phi_g(\mathbf{x}) \approx \phi_{\text{ho}}(x, y, z) = \frac{(\gamma_y \gamma_z)^{1/4}}{\pi^{3/4}} e^{-\frac{x^2 + \gamma_y y^2 + \gamma_z z^2}{2}}, \quad \mathbf{x} \in \mathbb{R}^3, \quad (2.1)$$

$$E_g \approx E(\phi_{\text{ho}}) = \frac{1}{2}(1 + \gamma_y + \gamma_z) + O(\beta), \quad |\beta| \ll 1, \quad (2.2)$$

$$\mu_g \approx \mu(\phi_{\text{ho}}) = \frac{1}{2}(1 + \gamma_y + \gamma_z) + O(\beta). \quad (2.3)$$

Regime II. Intermediate interacting regime, $\beta = O(1)$, the ground state can be obtained by solving the 3D minimization problem (1.9). Different numerical methods were proposed in the literatures for computing the ground states [7, 4, 3, 12, 13].

Regime III. Strong interacting regime, $\beta \gg 1$, noticing (A.7) and (A.6), the ground state is approximated by the Thomas-Fermi (TF) approximation [13, 15, 29, 7]:

$$\phi_g(\mathbf{x}) \approx \phi_g^{\text{TF}}(\mathbf{x}) = \begin{cases} \sqrt{(\mu_g^{\text{TF}} - V(\mathbf{x})) / \beta}, & V(\mathbf{x}) < \mu_g^{\text{TF}}, \\ 0, & \text{otherwise,} \end{cases} \quad (2.4)$$

$$\mu_g^{\text{TF}} = \frac{1}{2} \left(\frac{15\beta\gamma_y\gamma_z}{4\pi} \right)^{2/5}, \quad \beta \gg 1, \quad (2.5)$$

$$E_g \approx \frac{5}{7}\mu_g^{\text{TF}} + \frac{\tilde{C}_3}{\beta^{2/5}} (\ln \beta + G_3) = \frac{5}{7}\mu_g^{\text{TF}} + O\left(\frac{\ln \beta}{\beta^{2/5}}\right), \quad (2.6)$$

$$\mu_g \approx \mu_g^{\text{TF}} + \frac{\tilde{C}_3}{\beta^{2/5}} (\ln \beta + G_3) = \mu_g^{\text{TF}} + O\left(\frac{\ln \beta}{\beta^{2/5}}\right). \quad (2.7)$$

For $\gamma_y = \gamma_z = 1$, (2.6) and (2.7) were confirmed numerically in [7].

2.2 Disk-shaped condensation

In the case of disk shaped condensates, i.e. $\gamma_y = O(1)$ and $\gamma_z \gg 1$ ($\iff \omega_y \approx \omega_x$ and $\omega_z \gg \omega_x$), we set

$$\mu_g \approx \mu + \frac{\gamma_z}{2}, \quad \phi_g(\mathbf{x}) \approx \phi(x, y)\phi_{\text{ho}}(z) \quad \text{with } \phi_{\text{ho}}(z) = \frac{\gamma_z^{1/4}}{\pi^{1/4}} e^{-\frac{\gamma_z z^2}{2}}. \quad (2.8)$$

Plugging (2.8) into (1.5), multiplying both sides by $\phi_{\text{ho}}(z)$ and integrating over $z \in (-\infty, \infty)$, we get

$$\mu \phi(x, y) = -\frac{1}{2}\Delta\phi(x, y) + V_2(x, y)\phi(x, y) + \beta_2^a |\phi(x, y)|^2\phi(x, y), \quad (x, y) \in \mathbb{R}^2, \quad (2.9)$$

where

$$V_2(x, y) = \frac{1}{2} (x^2 + \gamma_y^2 y^2), \quad \beta_2^a = \beta \int_{-\infty}^{\infty} |\phi_{\text{ho}}(z)|^4 dz = \beta \sqrt{\frac{\gamma_z}{2\pi}}.$$

Using the results in Appendix A for 2D GPE, again we get approximate ground state in three typical regimes:

Regime I. Weakly interacting regime, i.e. $\beta_2^a = \beta \sqrt{\gamma_z/2\pi} = o(1)$, the ground state is approximated by the harmonic oscillator ground state:

$$\phi_g(\mathbf{x}) \approx \phi_{\text{ho}}(x, y)\phi_{\text{ho}}(z) = \phi_{\text{ho}}(x, y, z), \quad \mathbf{x} \in \mathbb{R}^3, \quad (2.10)$$

$$E_g \approx \frac{\gamma_z}{2} + \frac{1 + \gamma_y}{2} + O(\beta_2^a) = \frac{\gamma_z}{2} + \frac{1 + \gamma_y}{2} + O(\beta\gamma_z^{1/2}), \quad (2.11)$$

$$\mu_g \approx \frac{\gamma_z}{2} + \frac{1 + \gamma_y}{2} + O(\beta_2^a) = \frac{\gamma_z}{2} + \frac{1 + \gamma_y}{2} + O(\beta\gamma_z^{1/2}), \quad \gamma_z \gg 1 \ \& \ \beta_2^a = o(1). \quad (2.12)$$

$1/\gamma_z$	1/25	1/100	1/400	1/1600
$\beta = 1$	2.23E-3	9.97E-4	4.17E-4	1.68E-4
rate		0.58	0.63	0.65
$\beta = 10$	1.23E-2	4.72E-3	1.74E-3	5.80E-4
rate		0.70	0.72	0.80
$\beta = 100$	4.46E-2	1.64E-2	5.93E-3	2.13E-3
rate		0.72	0.73	0.74
$\beta = 1000$	1.38E-1	5.31E-2	1.94E-2	6.99E-3
rate		0.69	0.73	0.74
$\beta = 10000$	3.46E-1	1.58E-1	6.19E-2	2.27E-2
rate		0.56	0.68	0.72

Table 1: Error analysis of $\|\phi_g(\cdot) - \phi_g^{\text{DS}}(\cdot)\|_{L^2}$ for the ground state in 3D with a disk-shaped trap.

Regime II. Intermediate interacting regime, i.e. $\beta_2^a = O(1)$, the ground state can be approximated by

$$\phi_g(\mathbf{x}) \approx \phi_g^{\text{DS}}(\mathbf{x}) := \phi_g^{2\text{D}}(x, y)\phi_{\text{ho}}(z), \quad \mathbf{x} \in \mathbb{R}^3. \quad (2.13)$$

$$E_g \approx E_g^{\text{DS}} := E(\phi_g^{2\text{D}}(x, y)\phi_{\text{ho}}(z)) = \frac{\gamma_z}{2} + E_{2\text{D}}(\phi_g^{2\text{D}}) := \frac{\gamma_z}{2} + E_g^{2\text{D}}, \quad (2.14)$$

$$\mu_g \approx \mu_g^{\text{DS}} := \mu(\phi_g^{2\text{D}}(x, y)\phi_{\text{ho}}(z)) = \frac{\gamma_z}{2} + \mu_{2\text{D}}(\phi_g^{2\text{D}}) := \frac{\gamma_z}{2} + \mu_g^{2\text{D}}, \quad (2.15)$$

where

$$E_g^{2\text{D}} = \int_{\mathbb{R}^2} \left[\frac{1}{2} |\nabla \phi_g^{2\text{D}}|^2 + V_2(x, y) |\phi_g^{2\text{D}}|^2 + \frac{\beta_2^a}{2} |\phi_g^{2\text{D}}|^4 \right] dx dy,$$

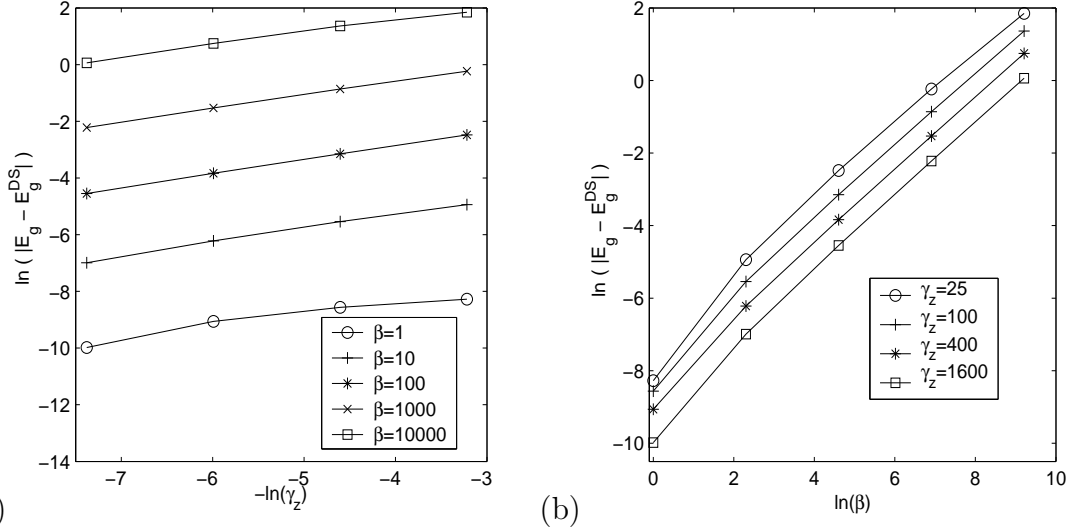
$$\mu_g^{2\text{D}} = \int_{\mathbb{R}^2} \left[\frac{1}{2} |\nabla \phi_g^{2\text{D}}|^2 + V_2(x, y) |\phi_g^{2\text{D}}|^2 + \beta_2^a |\phi_g^{2\text{D}}|^4 \right] dx dy.$$

Here $\phi_g^{2\text{D}}$, $E_g^{2\text{D}}$ and $\mu_g^{2\text{D}}$ are the ground state, energy and chemical potential of the 2D problem (2.9). In this case, one only needs to solve a 2D problem numerically and thus significantly save computational time, memory and cost.

To verify (2.13), (2.14) and (2.15) numerically, Table 1 list the error $\|\phi_g(\mathbf{x}) - \phi_g^{\text{DS}}(\mathbf{x})\|_{L^2}$, and Figure 1 shows the error and $|E_g - E_g^{\text{DS}}|$, with $\gamma_y = 1$ for different β and γ_z . Here and in the following, the ground state ϕ_g is computed numerically by the continuous normalized gradient flow (CNGF) with a backward Euler finite difference (BEFD) discretization [4].

From Tab. 1, Fig. 1 and additional numerical results [18], when $\gamma_z \gg 1$, $\beta_2^a = \beta\sqrt{\gamma_z/2\pi} = O(1)$ or $\gg 1$, and $\beta\gamma_z^{-3/2} = o(1)$, we can draw the following conclusion:

$$\|\phi_g - \phi_g^{\text{DS}}\|_{L^2} = O\left(\frac{\beta^{1/2} \ln \gamma_z}{\gamma_z^{3/4}}\right), \quad \|\phi_g^2 - (\phi_g^{\text{DS}})^2\|_{L^1} = O\left(\frac{\beta^{1/2} \ln \gamma_z}{\gamma_z^{3/4}}\right),$$



(a) (b)
Figure 1: Convergence rate of $|E_g - E_g^{\text{DS}}|$ in 3D with a disk-shaped trap: (a) With respect to γ_z ; (b) with respect to β .

$$|E_g - E_g^{\text{DS}}| = O\left(\frac{\beta \ln \gamma_z}{\gamma_z^{1/2}}\right), \quad |\mu_g - \mu_g^{\text{DS}}| = O\left(\frac{\beta \ln \gamma_z}{\gamma_z^{1/2}}\right).$$

On the contrary, when $\gamma_z \gg 1$, $\beta_2^a = \beta \sqrt{\gamma_z/2\pi} = O(1)$ or $\gg 1$, and $\beta \gamma_z^{-3/2} = O(1)$ or $\gg 1$, the errors do not decrease when γ_z increases. This suggests that one cannot reduce the 3D GPE (1.5) to 2D GPE (2.9) when $\beta \gg 1$ and $\gamma_z \gg 1$ with $\beta \gamma_z^{-3/2} = O(1)$ or $\gg 1$.

Regime III. Strong interacting regime, $\beta_2^a = \beta \sqrt{\gamma_z/2\pi} \gg 1$, noticing (A.17), the ground state is approximated by the multiplication of the TF approximation in xy -plane and the harmonic oscillator approximation in z -direction:

$$\phi_g(\mathbf{x}) \approx \phi_g^{\text{TF1}}(\mathbf{x}) := \phi_{2\text{D}}^{\text{TF}}(x, y) \phi_{\text{ho}}(z), \quad \mathbf{x} \in \mathbb{R}^3, \quad (2.16)$$

where

$$\phi_{2\text{D}}^{\text{TF}}(x, y) = \begin{cases} \sqrt{(\mu_{2\text{D}}^{\text{TF}} - V_2(x, y)) / \beta_2^a}, & V_2(x, y) < \mu_{2\text{D}}^{\text{TF}}, \\ 0 & \text{otherwise,} \end{cases} \quad (2.17)$$

$$\mu_{2\text{D}}^{\text{TF}} = \left(\frac{\beta_2^a \gamma_y}{\pi}\right)^{1/2} = \frac{\beta^{1/2} \gamma_y^{1/2} \gamma_z^{1/4}}{2^{1/4} \pi^{3/4}}. \quad (2.18)$$

Plugging (2.13), (2.9), (A.7) with $d = 2$, (2.18), (A.16) with $d = 2$ and $\beta_2 = \beta_2^a = \beta \sqrt{\frac{\gamma_z}{2\pi}}$ into (2.14), we get the approximate energy

$$E_g = E(\phi_g) = E(\phi_g^{2\text{D}}(x, y) \phi_{\text{ho}}(z)) + O\left(\frac{\beta \ln \gamma_z}{\gamma_z^{1/2}}\right)$$

$1/\gamma_z$	1/25	1/100	1/400	1/1600
$\beta = 1$	5.45E-1	4.44E-1	3.57E-1	2.88E-1
rate		0.15	0.16	0.15
$\beta = 10$	2.66E-1	2.15E-1	1.74E-1	1.40E-1
rate		0.15	0.16	0.15
$\beta = 100$	1.29E-1	1.03E-1	8.43E-2	6.77E-2
rate		0.16	0.14	0.16
$\beta = 1000$	1.40E-1	6.49E-2	4.12E-2	3.19E-2
rate		0.55	0.33	0.18

Table 2: Error analysis of $\|\phi_g - \phi^{\text{TF1}}\|_{L^2}$ for the ground state in 3D with a disk-shaped trap.

$$\begin{aligned}
&= \frac{\gamma_z}{2} + E_{2\text{D}}(\phi_g^{2\text{D}}) + O\left(\frac{\beta \ln \gamma_z}{\gamma_z^{1/2}}\right) = \frac{\gamma_z}{2} + E_g^{2\text{D}} + O\left(\frac{\beta \ln \gamma_z}{\gamma_z^{1/2}}\right) \\
&\approx \frac{\gamma_z}{2} + \frac{2}{3} \left(\frac{\beta_2^a \gamma_y}{\pi}\right)^{1/2} + \frac{\tilde{C}_2}{(\beta_2^a)^{1/2}} (\ln \beta_2^a + G_2) + O\left(\frac{\beta \ln \gamma_z}{\gamma_z^{1/2}}\right) \\
&\approx \frac{\gamma_z}{2} + \frac{2^{3/4} \gamma_y^{1/2} (\beta^2 \gamma_z)^{1/4}}{3\pi^{3/4}} + \frac{\tilde{C}_2 (2\pi)^{1/4}}{2(\beta^2 \gamma_z)^{1/4}} [\ln(\beta^2 \gamma_z) + 2G_2 - \ln 2\pi] + O\left(\frac{\beta \ln \gamma_z}{\gamma_z^{1/2}}\right) \\
&= E_g^{\text{TF1}} + O\left(\frac{\ln(\beta^2 \gamma_z)}{(\beta^2 \gamma_z)^{1/4}} + \frac{\beta \ln \gamma_z}{\gamma_z^{1/2}}\right), \tag{2.19}
\end{aligned}$$

where

$$E_g^{\text{TF1}} = \frac{\gamma_z}{2} + \frac{2^{3/4} \gamma_y^{1/2} (\beta^2 \gamma_z)^{1/4}}{3\pi^{3/4}}. \tag{2.20}$$

Similarly, we get the approximate chemical potential:

$$\mu_g \approx \mu_g^{\text{TF1}} + O\left(\frac{\ln(\beta^2 \gamma_z)}{(\beta^2 \gamma_z)^{1/4}} + \frac{\beta \ln \gamma_z}{\gamma_z^{1/2}}\right), \tag{2.21}$$

where

$$\mu_g^{\text{TF1}} = \frac{\gamma_z}{2} + \frac{\gamma_y^{1/2} (\beta^2 \gamma_z)^{1/4}}{2^{1/4} \pi^{3/4}}. \tag{2.22}$$

To verify (2.16), (2.19) and (2.21) numerically, Tables 2 and 3 list the errors $\|\phi_g(\mathbf{x}) - \phi^{\text{TF1}}(\mathbf{x})\|_{L^2}$ and $\|\phi_g(\mathbf{x}) - \phi^{\text{TF1}}(\mathbf{x})\|_{L^\infty}$, respectively, and Figure 2 shows the error $|E_g - E_g^{\text{TF1}}|$, with $\gamma_y = 1$ for different β and γ_z .

From Tabs. 2&3, Fig. 2 and additional numerical results in [18], when $\gamma_y = O(1)$, $\gamma_z \gg 1$, $\beta_2^a = \beta \sqrt{\gamma_z/2\pi} \gg 1$ and $\beta \gamma_z^{-3/2} = o(1)$, we can draw the following conclusion:

$$\|\phi_g - \phi^{\text{TF1}}\|_{L^2} = O\left(\frac{C(\beta) \ln \gamma_z}{\gamma_z^{1/4}}\right), \quad \|\phi_g^2 - (\phi^{\text{TF1}})^2\|_{L^1} = O\left(\frac{C(\beta) \ln \gamma_z}{\gamma_z^{1/4}}\right),$$

$1/\gamma_z$	1/25	1/100	1/400	1/1600
$\beta = 1$	0.3880	0.3148	0.3107	0.3749
$\beta = 10$	3.845E-2	4.589E-2	5.337E-2	6.198E-2
$\beta = 100$	6.368E-3	7.048E-3	8.597E-3	9.757E-3

Table 3: Error analysis of $\|\phi_g - \phi^{\text{TF1}}\|_{L^\infty}$ for the ground state in 3D with a disk-shaped trap.

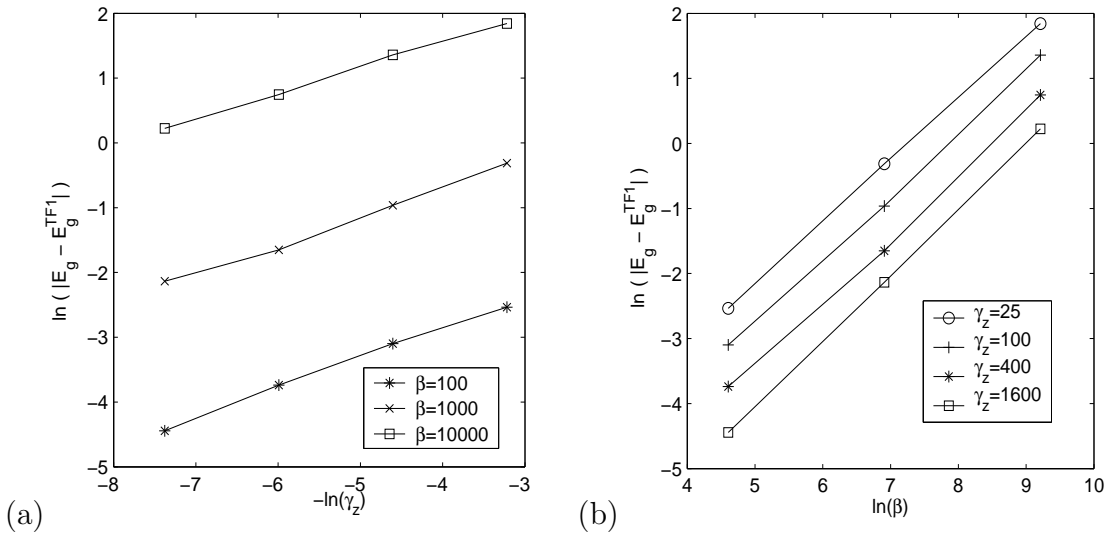


Figure 2: Convergence rate of $|E_g - E_g^{\text{TF1}}|$ in 3D with a disk-shaped trap: (a) With respect to γ_z ; (b) with respect to β .

$$|E_g - E_g^{\text{TF1}}| = O\left(\frac{C(\beta) \ln \gamma_z}{\gamma_z^{1/4}}\right), \quad |\mu_g - \mu_g^{\text{TF1}}| = O\left(\frac{C(\beta) \ln \gamma_z}{\gamma_z^{1/4}}\right),$$

where $C(\beta)$ depends on β . These results confirm the asymptotic results (2.19) and (2.21). Furthermore, the additional numerical results in [7, 18] indicate that $\phi^{\text{TF1}}(\mathbf{x})$ does not converge pointwise to the ground state $\phi_g(\mathbf{x})$ when $\gamma_z \rightarrow \infty$ and $\beta > 0$ (cf. Tab. 3).

2.3 Cigar-shaped condensation

In the case of cigar shaped condensates, i.e. $\gamma_y \gg 1$ and $\gamma_z \gg 1$ ($\iff \omega_y \gg \omega_x$ and $\omega_z \gg \omega_x$), we set

$$\mu_g \approx \mu + \frac{\gamma_y + \gamma_z}{2}, \quad \phi_g(\mathbf{x}) \approx \phi(x)\phi_{\text{ho}}(y, z), \quad \phi_{\text{ho}}(y, z) = \frac{(\gamma_y \gamma_z)^{1/4}}{\pi^{1/2}} e^{-\frac{\gamma_y y^2 + \gamma_z z^2}{2}}. \quad (2.23)$$

Plugging (2.23) into (1.5), multiplying both sides by $\phi_{\text{ho}}(y, z)$ and integrating over $(y, z) \in \mathbb{R}^2$, we get

$$\mu \phi(x) = -\frac{1}{2}\phi_{xx} + V_1(x)\phi + \beta_1^a |\phi|^2 \phi, \quad -\infty < x < \infty, \quad (2.24)$$

where

$$V_1(x) = \frac{x^2}{2}, \quad \beta_1^a = \beta \int_{\mathbb{R}^2} |\phi_{\text{ho}}(y, z)|^4 dydz = \frac{\beta \sqrt{\gamma_y \gamma_z}}{2\pi}.$$

Using the results in the Appendix A for 1D GPE, again we get approximate ground state in three typical regimes:

Regime I. Weakly interacting regime, i.e. $\beta_1^a = \beta \sqrt{\gamma_y \gamma_z} / 2\pi = o(1)$, the ground state is approximated by the harmonic oscillator ground state:

$$\phi_g(\mathbf{x}) \approx \phi_{\text{ho}}(x)\phi_{\text{ho}}(y, z) = \phi_{\text{ho}}(x, y, z), \quad \mathbf{x} \in \mathbb{R}^3, \quad \gamma_y \gg 1 \ \& \ \gamma_z \gg 1 \ \& \ \beta_1^a = o(1), \quad (2.25)$$

$$E_g \approx \frac{\gamma_y + \gamma_z}{2} + \frac{1}{2} + O(\beta_1^a) = \frac{\gamma_y + \gamma_z}{2} + \frac{1}{2} + O\left(\beta(\gamma_y \gamma_z)^{1/2}\right), \quad (2.26)$$

$$\mu_g \approx \frac{\gamma_y + \gamma_z}{2} + \frac{1}{2} + O(\beta_1^a) = \frac{\gamma_y + \gamma_z}{2} + \frac{1}{2} + O\left(\beta(\gamma_y \gamma_z)^{1/2}\right). \quad (2.27)$$

Regime II. Intermediate interacting regime, i.e. $\beta_1^a = \beta \sqrt{\gamma_y \gamma_z} / 2\pi = O(1)$, the ground state can be approximated by

$$\phi_g(\mathbf{x}) \approx \phi_g^{\text{CS}}(\mathbf{x}) := \phi_g^{\text{1D}}(x)\phi_{\text{ho}}(y, z), \quad \mathbf{x} \in \mathbb{R}^3, \quad (2.28)$$

$$E_g \approx E_g^{\text{CS}} := E(\phi_g^{\text{1D}}(x)\phi_{\text{ho}}(y, z)) = \frac{\gamma_y + \gamma_z}{2} + E_{\text{1D}}(\phi_g^{\text{1D}}) := \frac{\gamma_y + \gamma_z}{2} + E_g^{\text{1D}}, \quad (2.29)$$

$$\mu_g \approx \mu_g^{\text{CS}} := \mu(\phi_g^{\text{1D}}(x)\phi_{\text{ho}}(y, z)) = \frac{\gamma_y + \gamma_z}{2} + \mu_{\text{1D}}(\phi_g^{\text{1D}}) := \frac{\gamma_y + \gamma_z}{2} + \mu_g^{\text{1D}}, \quad (2.30)$$

where

$$E_g^{\text{1D}} = \int_{-\infty}^{\infty} \left[\frac{1}{2} \left| \frac{d\phi_g^{\text{1D}}(x)}{dx} \right|^2 + V_1(x) |\phi_g^{\text{1D}}(x)|^2 + \frac{\beta_1^a}{2} |\phi_g^{\text{1D}}(x)|^4 \right] dx,$$

$$\mu_g^{\text{1D}} = \int_{-\infty}^{\infty} \left[\frac{1}{2} \left| \frac{d\phi_g^{\text{1D}}(x)}{dx} \right|^2 + V_1(x) |\phi_g^{\text{1D}}(x)|^2 + \beta_1^a |\phi_g^{\text{1D}}(x)|^4 \right] dx.$$

Here ϕ_g^{1D} , E_g^{1D} and μ_g^{1D} are the ground state, energy and chemical potential of the 1D problem (2.24). In this case, one only needs to solve a 1D problem numerically and thus significantly save computational time, memory and cost.

To verify (2.13), (2.14) and (2.15) numerically, Table 4 lists the error $\|\phi_g(\mathbf{x}) - \phi_g^{\text{CS}}(\mathbf{x})\|_{L^2}$, and Figure 3 shows the error $\frac{|E_g - E_g^{\text{CS}}|}{E_g}$, for different β and $\gamma := \gamma_y = \gamma_z$.

$1/\gamma$	1/12.5	1/25	1/50	1/100	1/200
$\beta = 25$	0.1512	0.1283	0.1076	0.0895	0.074
rate		0.24	0.25	0.27	0.28
$\beta = 50$	0.2232	0.1914	0.1162	0.1363	0.1136
rate		0.22	0.24	0.25	0.26
$\beta = 100$	0.3150	0.2742	0.2357	0.2006	0.1692
rate		0.20	0.22	0.23	0.25
$\beta = 200$	0.4228	0.3740	0.3269	0.2826	0.2418
rate		0.18	0.19	0.21	0.22
$\beta = 400$	0.5389	0.4851	0.4316	0.3798	0.3309
rate		0.15	0.17	0.18	0.20

Table 4: Error analysis of $\|\phi_g - \phi_g^{\text{CS}}\|_{L^2}$ for the ground state in 3D with a cigar-shaped trap.

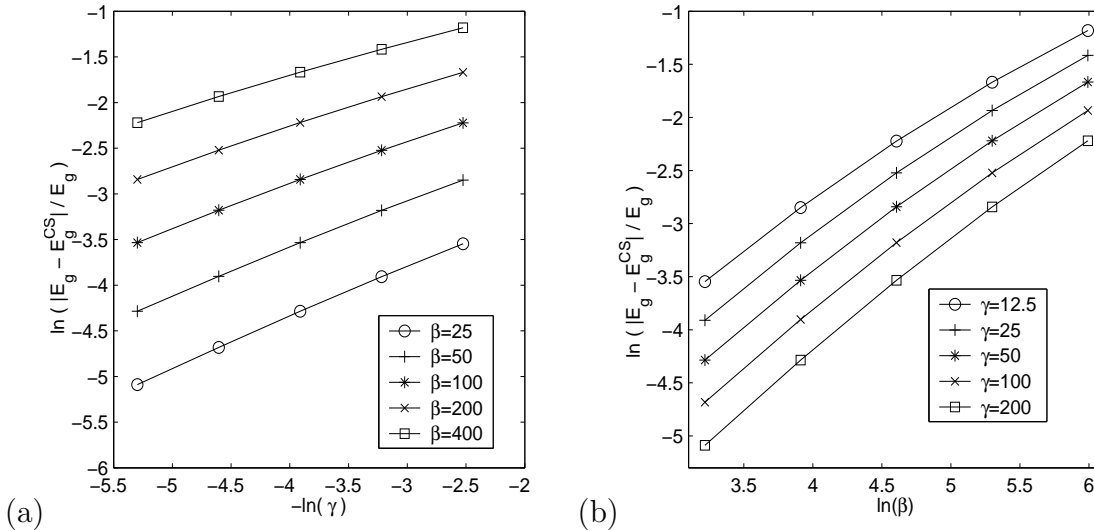


Figure 3: Convergence rate of $\frac{|E_g - E_g^{\text{CS}}|}{E_g}$ in 3D with a cigar-shaped trap: (a) With respect to γ ; (b) with respect to β .

From Tab. 4, Fig. 3 and additional numerical results in [18], when $\gamma = \gamma_y = \gamma_z \gg 1$, $\beta_1^a = \beta\gamma/2\pi = O(1)$ or $\gg 1$, and $\beta\gamma^{-1} = o(1)$, we can draw the following conclusion:

$$\|\phi_g^2 - (\phi_g^{\text{CS}})^2\|_{L^1} = O\left(\frac{\beta^{1/3} \ln \gamma}{\gamma^{1/3}}\right), \quad \|\phi_g - \phi_g^{\text{CS}}(x)\|_{L^2} = O\left(\frac{\beta^{1/3} \ln \gamma}{\gamma^{1/3}}\right),$$

$$|E_g - E_g^{\text{CS}}| = O\left(\beta \gamma^{1/3} \ln \gamma\right), \quad \frac{|E_g - E_g^{\text{CS}}|}{E_g} = O\left(\frac{\beta^{1/3} \ln \gamma}{\gamma^{2/3}}\right),$$

$$|\mu_g - \mu_g^{\text{CS}}| = O\left(\beta \gamma^{1/3} \ln \gamma\right), \quad \frac{|\mu_g - \mu_g^{\text{CS}}|}{\mu_g} = O\left(\frac{\beta^{1/3} \ln \gamma}{\gamma^{2/3}}\right).$$

On the contrary, when $\gamma = \gamma_y = \gamma_z \gg 1$, $\beta_1^a = \beta\gamma/2\pi = O(1)$ or $\gg 1$, and $\beta\gamma^{-1} = O(1)$ or $\gg 1$, the errors do not decrease when γ increases. This suggests that one cannot reduce the 3D GPE (1.5) to 1D GPE (2.24) when $\beta \gg 1$ and $\gamma \gg 1$ with $\beta\gamma^{-1} = O(1)$ or $\gg 1$.

Regime III. Strong interacting regime, $\beta_1^a = \beta\sqrt{\gamma_y\gamma_z}/2\pi \gg 1$, noticing (A.17) with $d = 1$, the ground state in 3D is approximated by the multiplication of the TF approximation in x -direction and the harmonic oscillator approximation in yz -plane:

$$\phi_g(\mathbf{x}) \approx \phi_g^{\text{TF2}}(\mathbf{x}) := \phi_{\text{1D}}^{\text{TF}}(x)\phi_{\text{ho}}(y, z), \quad \mathbf{x} \in \mathbb{R}^3, \quad (2.31)$$

where

$$\phi_{\text{1D}}^{\text{TF}}(x) = \begin{cases} \sqrt{(\mu_{\text{1D}}^{\text{TF}} - x^2/2)/\beta_1^a}, & x^2 < 2\mu_{\text{1D}}^{\text{TF}}, \\ 0 & \text{otherwise,} \end{cases} \quad (2.32)$$

$$\mu_{\text{1D}}^{\text{TF}} = \frac{1}{2} \left(\frac{3\beta_1^a}{2} \right)^{2/3} = \frac{(3\beta)^{2/3}(\gamma_y\gamma_z)^{1/3}}{2(4\pi)^{2/3}}. \quad (2.33)$$

Plugging (2.28), (2.24), (A.7) with $d = 1$, (2.33), (A.16) with $d = 1$ and $\beta_1 = \beta_1^a$ into (2.14), we get the approximate energy:

$$\begin{aligned} E_g &= E(\phi_g) = E_g(\phi_g^{\text{1D}}(x)\phi_{\text{ho}}(y, z)) + O\left(\beta\gamma_y^{1/3} \ln \gamma_y\right) \\ &= \frac{\gamma_y + \gamma_z}{2} + E_{\text{1D}}(\phi_g^{\text{1D}}) + O\left(\beta\gamma_y^{1/3} \ln \gamma_y\right) = \frac{\gamma_y + \gamma_z}{2} + E_g^{\text{1D}} + O\left(\beta\gamma_y^{1/3} \ln \gamma_y\right) \\ &\approx \frac{\gamma_y + \gamma_z}{2} + \frac{3}{5} \frac{1}{2} \left(\frac{3\beta_1^a}{2} \right)^{2/3} + \frac{\tilde{C}_1}{(\beta_1^a)^{2/3}} (\ln \beta_1^a + G_1) + O\left(\beta\gamma_y^{1/3} \ln \gamma_y\right) \\ &\approx E_g^{\text{TF2}} + O\left(\beta\gamma_y^{1/3} \ln \gamma_y\right), \end{aligned} \quad (2.34)$$

where

$$E_g^{\text{TF2}} = \frac{\gamma_y + \gamma_z}{2} + \frac{3^{5/3}(\beta^2\gamma_y\gamma_z)^{1/3}}{10(4\pi)^{2/3}}. \quad (2.35)$$

Similarly, we get the approximate chemical potential:

$$\mu_g \approx \mu_g^{\text{TF2}} + O\left(\beta\gamma_y^{1/3} \ln \gamma_y\right), \quad (2.36)$$

where

$$\mu_g^{\text{TF2}} = \frac{\gamma_y + \gamma_z}{2} + \frac{3^{2/3}(\beta^2\gamma_y\gamma_z)^{1/3}}{2(4\pi)^{2/3}}. \quad (2.37)$$

Specifically, if $\gamma_y = \gamma_z := \gamma$, then (2.33), (2.34) and (2.36) collapse to

$$E_g \approx E_g^{\text{TF2}} + O\left(\beta\gamma^{1/3} \ln \gamma\right), \quad \mu_g \approx \mu_g^{\text{TF2}} + O\left(\beta\gamma^{1/3} \ln \gamma\right), \quad (2.38)$$

$$\mu_{\text{1D}}^{\text{TF}} = \frac{(3\beta\gamma)^{2/3}}{2(4\pi)^{2/3}}, \quad E_g^{\text{TF2}} = \gamma + \frac{3^{5/3}(\beta\gamma)^{2/3}}{10(4\pi)^{2/3}}, \quad \mu_g^{\text{TF2}} = \gamma + \frac{3^{2/3}(\beta\gamma)^{2/3}}{2(4\pi)^{2/3}}. \quad (2.39)$$

$1/\gamma_z$	1/12.5	1/25	1/50	1/100	1/400
$\beta = 25$	0.2360	0.1958	0.1606	0.1309	0.1061
rate		0.27	0.29	0.30	0.30
$\beta = 50$	0.3385	0.2851	0.2373	0.1958	0.1604
rate		0.25	0.26	0.28	0.29
$\beta = 100$	0.4691	0.4022	0.3407	0.2857	0.2375
rate		0.22	0.24	0.25	0.27
$\beta = 200$	0.6212	0.5440	0.4706	0.4026	0.3408
rate		0.19	0.21	0.23	0.24
$\beta = 400$	0.7856	0.7031	0.6221	0.5442	0.4707
rate		0.16	0.18	0.19	0.21

Table 5: Error analysis of $\|\phi_g^2 - (\phi_g^{\text{TF2}}(\mathbf{x}))^2\|_{L^1}$ for the ground state in 3D with a cigar-shaped trap.

$1/\gamma_z$	1/12.5	1/25	1/50	1/100	1/200
$\beta = 25$	0.1226	0.1447	0.1711	0.2025	0.2390
$\beta = 50$	0.1633	0.1985	0.2402	0.2880	0.3426
$\beta = 100$	0.2110	0.2597	0.3158	0.3794	0.4516
$\beta = 200$	0.2517	0.3100	0.3769	0.4531	0.5393
$\beta = 400$	0.2772	0.3410	0.4146	0.5001	0.5975

Table 6: Error analysis of $\|\phi_g - \phi^{\text{TF2}}\|_{L^\infty}$ for the ground state in 3D with a disk-shaped trap.

To verify (2.31), (2.38) and (2.39) numerically, Tables 5 and 6 list the errors $\|\phi_g^2(\mathbf{x}) - (\phi_g^{\text{TF2}}(\mathbf{x}))^2\|_{L^1}$ and $\|\phi_g^2(\mathbf{x}) - (\phi_g^{\text{TF2}}(\mathbf{x}))^2\|_{L^\infty}$, respectively, and Figure 4 shows the error $\frac{|E_g - E_g^{\text{TF2}}|}{E_g}$, for different β and γ .

From Tabs. 5-6, Fig. 4 and additional numerical results in [18], when $\gamma := \gamma_y = \gamma_z \gg 1$, $\beta_1^a = \beta\gamma/2\pi \gg 1$ and $\beta\gamma^{-1} = o(1)$, we can draw the following conclusion:

$$\begin{aligned}
\|\phi_g - \phi_g^{\text{TF2}}\|_{L^2} &= O\left(\frac{\beta^{1/3} \ln \gamma}{\gamma^{1/3}}\right), & \|\phi_g^2 - (\phi_g^{\text{TF2}})^2\|_{L^1} &= O\left(\frac{\beta^{1/3} \ln \gamma}{\gamma^{1/3}}\right), \\
|E_g - E_g^{\text{TF2}}| &= O\left(\beta \gamma^{1/3} \ln \gamma\right), & \frac{|E_g - E_g^{\text{TF2}}|}{E_g} &= O\left(\frac{\beta^{1/3} \ln \gamma}{\gamma^{2/3}}\right), \\
|\mu_g - \mu_g^{\text{TF2}}| &= O\left(\beta \gamma^{1/3} \ln \gamma\right), & \frac{|\mu_g - \mu_g^{\text{TF2}}|}{\mu_g} &= O\left(\frac{\beta^{1/3} \ln \gamma}{\gamma^{2/3}}\right).
\end{aligned}$$

These results confirm the asymptotic results (2.38), (2.39), (2.34) and (2.36). Furthermore, the additional numerical results in [7, 18] indicate that $\phi_g^{\text{TF2}}(\mathbf{x})$ does not

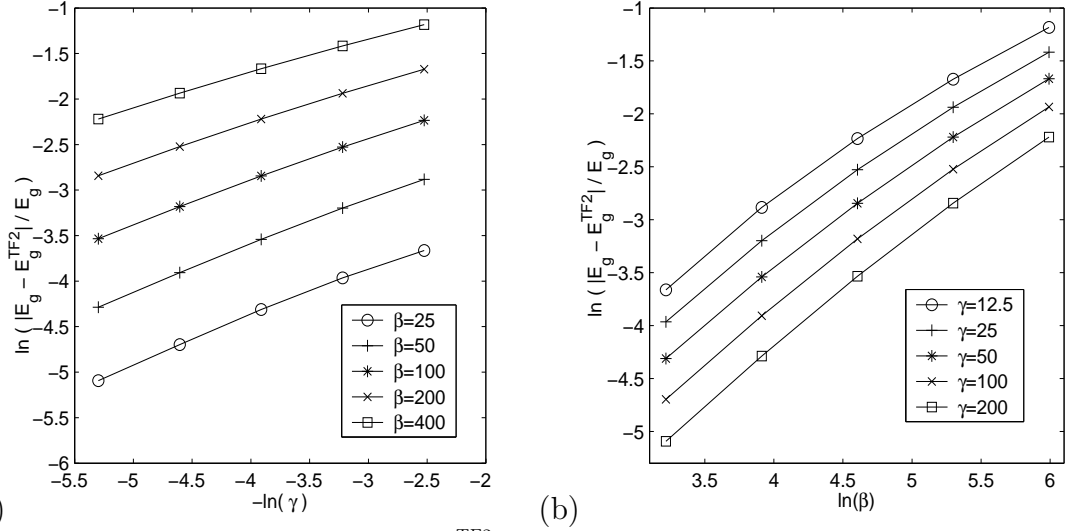


Figure 4: Convergence rate of $\frac{|E_g - E_g^{\text{TF2}}|}{E_g}$ in 3D with a cigar-shaped trap: (a) With respect to γ ; (b) with respect to β .

converge pointwise to the ground state $\phi_g(\mathbf{x})$ when $\gamma_z \rightarrow \infty$ and $\beta > 0$ (cf. Tab. 6).

2.4 Choice of initial data for computing ground states of 3D GPE

In order to numerically compute the ground state of the 3D GPE (1.5) efficiently, for a given numerical method, an appropriate choice of the initial data is also very important such that the iterative number is highly reduced and thus the total computational cost is greatly saved [7, 4, 13]. Based on the discussion in the previous subsections, here we provide an appropriate choice for the initial data for different parameter regimes β , γ_y and γ_z in (1.5):

- I. When i) $\gamma_y = O(1)$, $\gamma_z = O(1)$ and $\beta = o(1)$ or $O(1)$; ii) $\gamma_y = O(1)$, $\gamma_z \gg 1$ and $\beta_2^a = \beta \sqrt{\gamma_z/2\pi} = o(1)$; or iii) $\gamma_y \gg 1$, $\gamma_z \gg 1$ and $\beta_1^a = \beta \sqrt{\gamma_y \gamma_z}/2\pi = o(1)$; an appropriate choice of the initial data is

$$\phi_0(\mathbf{x}) = \phi_{\text{ho}}(x, y, z) = \frac{(\gamma_y \gamma_z)^{1/4}}{\pi^{3/4}} e^{-\frac{x^2 + \gamma_y y^2 + \gamma_z z^2}{2}}, \quad \mathbf{x} \in \mathbb{R}^3.$$

- II. When $\gamma_y = O(1)$, $\gamma_z \gg 1$, $\beta_2^a = \beta \sqrt{\gamma_z/2\pi} = O(1)$ and $\beta \gamma_z^{-3/2} = o(1)$, an appropriate choice of the initial data is

$$\phi_0(\mathbf{x}) = \phi_g^{2\text{D}}(x, y) \phi_{\text{ho}}(z) = \frac{\gamma_z^{1/4}}{\pi^{1/4}} e^{-\frac{\gamma_z z^2}{2}} \phi_g^{2\text{D}}(x, y), \quad \mathbf{x} \in \mathbb{R}^3;$$

where $\phi_g^{2\text{D}}(x, y)$ is the ground state of the 2D GPE (2.9) and can be computed numerically [7, 4, 13].

- III. When $\gamma_y = O(1)$, $\gamma_z \gg 1$, $\beta_2^a = \beta\sqrt{\gamma_z/2\pi} \gg 1$ and $\beta\gamma_z^{-3/2} = o(1)$, an appropriate choice of the initial data is

$$\phi_0(\mathbf{x}) = \phi_{2D}^{\text{TF}}(x, y) \phi_{\text{ho}}(z) = \frac{\gamma_z^{1/4}}{\pi^{1/4}} e^{-\frac{\gamma_z z^2}{2}} \phi_{2D}^{\text{TF}}(x, y), \quad \mathbf{x} \in \mathbb{R}^3;$$

where $\phi_{2D}^{\text{TF}}(x, y)$ is given in (2.17).

- IV. When $\gamma_y \gg 1$, $\gamma_z \gg 1$, $\beta_1^a = \beta\sqrt{\gamma_y\gamma_z}/2\pi = O(1)$ and $\beta(\gamma_y\gamma_z)^{-1/2} = o(1)$, an appropriate choice of the initial data is

$$\phi_0(\mathbf{x}) = \phi_g^{\text{1D}}(x) \phi_{\text{ho}}(y, z) = \frac{(\gamma_y\gamma_z)^{1/4}}{\pi^{1/2}} e^{-\frac{\gamma_y y^2 + \gamma_z z^2}{2}} \phi_g^{\text{1D}}(x), \quad \mathbf{x} \in \mathbb{R}^3;$$

where $\phi_g^{\text{1D}}(x)$ is the ground state of the 1D GPE (2.24) and can be computed numerically [7, 4, 13].

- V. When $\gamma_y \gg 1$, $\gamma_z \gg 1$, $\beta_1^a = \beta\sqrt{\gamma_y\gamma_z}/2\pi \gg 1$ and $\beta(\gamma_y\gamma_z)^{-1/2} = o(1)$, an appropriate choice of the initial data is

$$\phi_0(\mathbf{x}) = \phi_{\text{1D}}^{\text{TF}}(x) \phi_{\text{ho}}(y, z) = \frac{(\gamma_y\gamma_z)^{1/4}}{\pi^{1/2}} e^{-\frac{\gamma_y y^2 + \gamma_z z^2}{2}} \phi_{\text{1D}}^{\text{TF}}(x), \quad \mathbf{x} \in \mathbb{R}^3;$$

where $\phi_{\text{1D}}^{\text{TF}}(x)$ is given in (2.32).

- VI. For all other cases, a good choice of the initial data is

$$\phi_0(\mathbf{x}) = \phi_g^{\text{TF}}(\mathbf{x}), \quad \mathbf{x} \in \mathbb{R}^3;$$

where $\phi_g^{\text{TF}}(\mathbf{x})$ is given in (2.4). In fact, in these cases, the 3D GPE (1.5) cannot be reduced to lower dimensions!

Our numerical experiments showed that the initial data in cases II-V are much better than initial data often used in the current literatures.

3 Dimension reduction for time-dependent GPE

In this section, we will discuss dimension reduction of the 3D time-dependent GPE (1.3) in certain limiting frequency regimes and provide convergence rate of the reduction based on our numerical results.

3.1 In disk-shaped condensates

In the disk-shaped condensates, i.e. for $\omega_x \approx \omega_y$ and $\omega_z \gg \omega_x$ ($\iff \gamma_y \approx 1$ and $\gamma_z \gg 1$), the 3D GPE (1.3) can be reduced to 2D GPE by assuming that the time evolution does not cause excitations along the z -axis since they have a larger energy of at least approximately $\hbar\omega_z$ compared to excitations along the x - and y -axis with

$1/\gamma_z$	1/25	1/100	1/400	1/1600
$\beta = 1$	1.954E-3	8.619E-4	3.547E-4	1.346E-4
rate		0.59	0.64	0.70
$\beta = 10$	1.056E-2	3.968E-3	1.446E-3	5.149E-4
rate		0.71	0.73	0.74
$\beta = 100$	3.709E-2	1.339E-2	4.769E-3	1.689E-3
rate		0.74	0.75	0.75
$\beta = 1000$	1.132E-1	4.216E-2	1.511E-2	5.364E-3
rate		0.71	0.74	0.75
$\beta = 10000$	2.902E-1	1.256E-1	4.707E-2	1.687E-2
rate		0.60	0.71	0.74

Table 7: Error analysis of $\|\phi_3 - \phi_{\text{ho}}\|_{L^2}$ for dimension reduction from 3D to 2D.

energies of about $\hbar\omega_x$. Following the physics literature [23, 17, 7, 5, 21], for any fixed $\beta \geq 0$ and when $\gamma_z \rightarrow \infty$, we assume that the condensation wave function along the z -axis is always well described by the ground state wave function which is well approximated by the harmonic oscillator in z -direction and set [21, 17, 7, 5]

$$\psi = \psi_2(x, y, t)\phi_3(z), \quad \phi_3(z) = \left(\int_{\mathbb{R}^2} |\phi_g(\mathbf{x})|^2 dx dy \right)^{1/2} \approx \phi_{\text{ho}}(z) = \frac{\gamma_z^{1/4}}{\pi^{1/4}} e^{-\gamma_z z^2/2}, \quad (3.1)$$

where $\phi_g(x, y, z)$ defined in (1.9) is the ground state solution of the 3D GPE (1.3). Following the procedure used in [21, 17], the 3D GPE (1.3) can be reduced to a 2D GPE with $\mathbf{x} = (x, y)$:

$$i \frac{\partial \psi(\mathbf{x}, t)}{\partial t} = -\frac{1}{2} \nabla^2 \psi(\mathbf{x}, t) + V_2(x, y) \psi(\mathbf{x}, t) + \beta_2 |\psi(\mathbf{x}, t)|^2 \psi(\mathbf{x}, t), \quad (3.2)$$

where

$$\beta_2 = \beta \int_{-\infty}^{\infty} \phi_3^4(z) dz \approx \beta_2^a := \beta \sqrt{\frac{\gamma_z}{2\pi}}, \quad V_2(x, y) = \frac{1}{2} (x^2 + \gamma_y^2 y^2). \quad (3.3)$$

To verify (3.1) and (3.3) numerically, Table 7 lists the error $\|\phi_3(z) - \phi_{\text{ho}}(z)\|_{L^2}$, and Figure 5 shows the error $\frac{|\beta_2 - \beta_2^a|}{\beta_2}$ vs. γ_z and β , for different β and γ_z .

From Tab. 7, Fig. 5 and additional numerical results in [18], for fixed $\beta \geq 0$ and when $\gamma_z \rightarrow \infty$, we can draw the following conclusion:

$$\begin{aligned} \beta_2 &= \beta \sqrt{\frac{\gamma_z}{2\pi}} \left(1 + O\left(\frac{\beta^{1/2} \ln \gamma_z}{\gamma_z^{3/4}}\right) \right), \quad \frac{|\beta_2 - \beta_2^a|}{\beta_2} = O\left(\frac{\beta^{1/2} \ln \gamma_z}{\gamma_z^{3/4}}\right), \\ \|\phi_3(z) - \phi_{\text{ho}}(z)\|_{L^2} &= O\left(\frac{\beta^{1/2} \ln \gamma_z}{\gamma_z^{3/4}}\right), \\ \|\phi_3^2(z) - \phi_{\text{ho}}^2(z)\|_{L^\infty} &= O\left(\frac{\beta^{1/2} \ln \gamma_z}{\gamma_z^{1/2}}\right), \quad \|\phi_3^2(z) - \phi_{\text{ho}}^2(z)\|_{L^1} = O\left(\frac{\beta^{1/2} \ln \gamma_z}{\gamma_z^{3/4}}\right). \end{aligned}$$

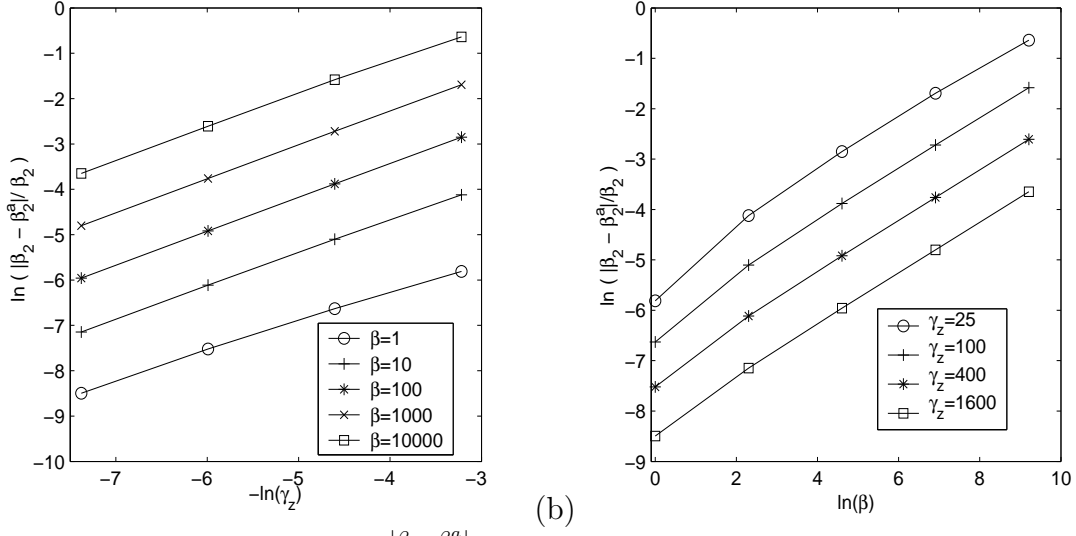


Figure 5: Convergence rate of $\frac{|\beta_2 - \beta_2^a|}{\beta_2}$ for dimension reduction from 3D to 2D: (a) With respect to γ_z ; (b) with respect to β .

In addition, we compare the errors between the solutions of the 3D GPE (1.3) and its 2D reduction (3.2) for different γ_z . In order to do so, for any given γ_z , let $\psi^{3D}(x, y, z, t)$ be the numerical solution of the 3D GPE (1.3) with $\gamma_x = \gamma_y = 2$, $\beta = 1$ and the initial data $\psi(x, y, z, 0) = \psi_0(x, y, z)$ chosen as the ground state of (1.3) with $\gamma_x = \gamma_y = 1$, $\beta = 1$ [4, 7]. This 3D dynamics corresponds to a BEC which is in its ground state when at $t = 0$ the trap frequencies in x and y direction are suddenly doubled, i.e. setting $\gamma_x = \gamma_y = 2$. Similarly, let $\psi^{2D}(x, y, t)$ be the numerical solution of the 2D GPE (3.2) with $\gamma_x = 2$, $\gamma_y = 2$, $\beta_2 = \beta_2^a := \beta \sqrt{\frac{\gamma_z}{2\pi}}$ and initial data $\psi(x, y, 0) = \psi_0(x, y)$ chosen as the ground state of (3.2) with $\gamma_x = \gamma_y = 1$, $\beta_2 = \beta_2^a = \beta \sqrt{\frac{\gamma_z}{2\pi}}$ [4, 7]. Again, this 2D dynamics corresponds to a BEC which is in its ground state when at $t = 0$ the trap frequencies in x and y direction are suddenly doubled, i.e. setting $\gamma_x = \gamma_y = 2$. In fact, ψ^{2D} is the solution of the 2D reduction problem. In order to do the comparison, we introduce

$$\phi_3(z, t) = \left(\int_{\mathbb{R}^2} |\psi^{3D}(x, y, z, t)|^2 dx dy \right)^{1/2} \approx \phi_{ho}(z) = \frac{\gamma_z^{1/4}}{\pi^{1/4}} e^{-\frac{\gamma_z z^2}{2}}, \quad (3.4)$$

$$\phi^{3D}(\mathbf{x}, t) \approx \phi^{DS}(\mathbf{x}, t) := \psi^{2D}(x, y, t) \phi_{ho}(z), \quad \mathbf{x} \in \mathbb{R}^3, \quad (3.5)$$

and the condensate widths

$$\sigma_\alpha(t) = \int_{\mathbb{R}^3} \alpha^2 |\psi^{3D}(\mathbf{x}, t)|^2 d\mathbf{x}, \quad \sigma_\alpha^a(t) = \int_{\mathbb{R}^3} \alpha^2 |\psi^{DS}(\mathbf{x}, t)|^2 d\mathbf{x}, \quad \alpha = x, y, z. \quad (3.6)$$

Figure 6 shows the errors $\|\psi_3(z, t) - \phi_{ho}(z)\|_{L^\infty}$, $|\sigma_x - \sigma_x^a| = |\sigma_y - \sigma_y^a|$, $\sigma_z - \sigma_z^a = \sigma_z - \frac{1}{4}$ and $\left| |\psi^{3D}(\mathbf{0}, t)|^2 - |\psi^{DS}(\mathbf{0}, t)|^2 \right|$ for different γ_z . Here the numerical solution ψ^{3D} and ψ^{2D} are obtained by the time splitting spectral method [5, 3].

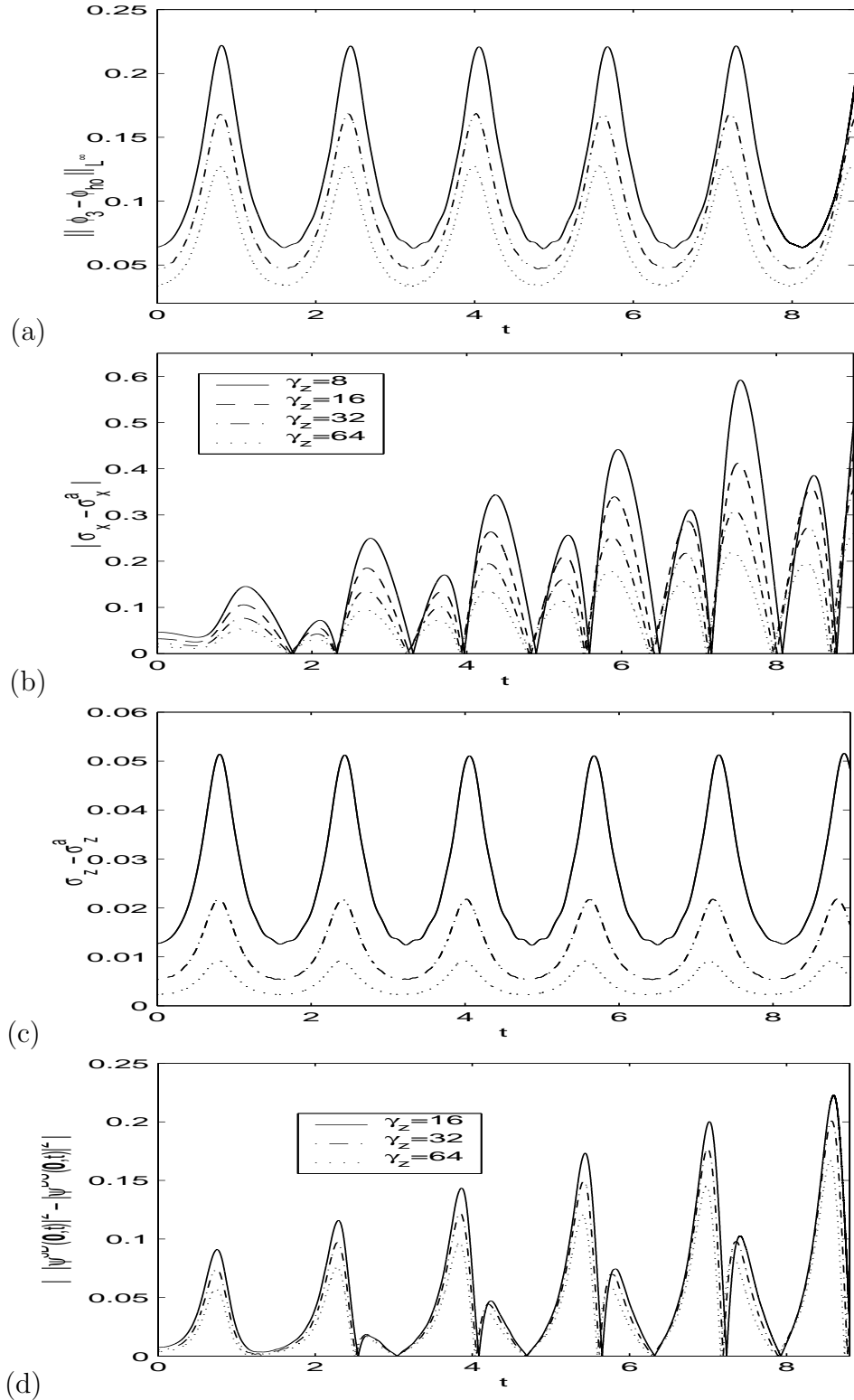


Figure 6: Convergence study for dimension reduction from 3D time-dependent GPE to 2D GPE.

From Fig. 6, the dimension reduction from 3D time-dependent GPE (1.3) to 2D GPE (3.2) when $\beta = O(1)$ and $\gamma_z \gg 1$ is verified numerically. Furthermore, we have the following convergence rate:

$$\begin{aligned} \|\phi_3(z, t) - \phi_{\text{ho}}(z)\|_{L^\infty} &= O\left(\frac{1}{\gamma_z^{3/4}}\right), & \sigma_x(t) &= \sigma_x^a(t) + O\left(\frac{1}{\gamma_z^{3/4}}\right), & \gamma_z &\gg 1, \\ \sigma_z(t) &= \frac{1}{4} + O\left(\frac{1}{\gamma_z^{3/4}}\right), & |\psi^{3\text{D}}(\mathbf{x}, t)|^2 &= |\psi^{\text{DS}}(\mathbf{x}, t)|^2 + O\left(\frac{1}{\gamma_z^{1/2}}\right). \end{aligned}$$

3.2 In cigar-shaped condensates

Similarly, in the cigar-shaped condensates, i.e. $\omega_y \gg \omega_x$ and $\omega_z \gg \omega_x$ ($\iff \gamma_y \gg 1$ and $\gamma_z \gg 1$), for any fixed $\beta \geq 0$ and when $\gamma_y \rightarrow \infty$ and $\gamma_z \rightarrow \infty$, the 3D GPE (1.3) can be reduced to 1D GPE with $\mathbf{x} = x$ [21, 23, 5, 7, 17]:

$$i \frac{\partial \psi(x, t)}{\partial t} = -\frac{1}{2} \partial_{xx} \psi(x, t) + V_1(x) \psi(x, t) + \beta_1 |\psi(x, t)|^2 \psi(x, t), \quad (3.7)$$

where

$$\beta_1 = \beta \int_{\mathbb{R}^2} |\phi_{23}(y, z)|^4 dy dz \approx \beta_1^a := \beta \frac{\sqrt{\gamma_y \gamma_z}}{2\pi}, \quad V_1(x) = \frac{x^2}{2}, \quad (3.8)$$

$$\phi_{23}(y, z) = \left(\int_{-\infty}^{\infty} |\phi_g(x, y, z)|^2 dx \right)^{1/2} \approx \phi_{\text{ho}}(y, z) := \frac{(\gamma_y \gamma_z)^{1/4}}{(\pi)^{1/2}} e^{-\frac{\gamma_y y^2 + \gamma_z z^2}{2}}. \quad (3.9)$$

Similarly, to verify (3.8) and (3.9) numerically with $\gamma := \gamma_y = \gamma_z$, Table 8 lists the error $\frac{\|\phi_{23}(y, z) - \phi_{\text{ho}}(y, z)\|_{L^\infty}}{\|\phi_{23}(y, z)\|_{L^\infty}}$, and Figure 7 shows the errors $\frac{|\beta_1 - \beta_1^a|}{\beta_1}$ vs. γ and β , for different γ and β .

From Tab. 8, Fig. 7 and additional numerical results in [18], for any fixed $\beta = O(1)$ and when $\gamma := \gamma_y = \gamma_z \rightarrow \infty$, we can draw the following conclusion:

$$\begin{aligned} \beta_1 &= \beta \frac{\gamma}{2\pi} \left(1 + O\left(\frac{\beta^{1/3} \ln \gamma}{\gamma^{1/3}}\right) \right), & \frac{|\beta_1 - \beta_1^a|}{\beta_1} &= O\left(\frac{\beta^{1/3} \ln \gamma}{\gamma^{1/3}}\right), \\ \|\phi_{23}(\cdot) - \phi_{\text{ho}}(\cdot)\|_{L^\infty} &= O\left(\beta^{1/3} \gamma^{1/3} \ln \gamma\right), & \frac{\|\phi_{23}(\cdot) - \phi_{\text{ho}}(\cdot)\|_{L^\infty}}{\|\phi_{23}(\cdot)\|_{L^\infty}} &= O\left(\frac{\beta^{1/3} \ln \gamma}{\gamma^{1/3}}\right), \\ \|\phi_{23}^2(\cdot) - \phi_{\text{ho}}^2(\cdot)\|_{L^1} &= O\left(\beta^{1/3} \gamma^{1/3} \ln \gamma\right), & \frac{\|\phi_{23}^2(\cdot) - \phi_{\text{ho}}^2(\cdot)\|_{L^1}}{\|\phi_{23}^2(\cdot)\|_{L^1}} &= O\left(\frac{\beta^{1/3} \ln \gamma}{\gamma^{1/3}}\right). \end{aligned}$$

3.3 For vortex interaction in 3D

In this subsection, we numerically study dimension reduction for vortex interaction in 3D disk-shaped condensates. In this case, the assumption $\phi_3(z) \approx \phi_{\text{ho}}(z)$ in (3.1) is no longer valid. In order to do so, for any given γ_z , let $\phi_1^{3\text{D}}(x, y, z)$ be the central vortex line state with winding number $m = 1$ of the 3D GPE (1.3) with $\gamma_x = \gamma_y = 1$

$1/\gamma$	1/12.5	1/25	1/50	1/100	1/400
$\beta = 25$	0.1727	0.1412	0.1145	0.0924	0.0743
rate		0.29	0.30	0.31	0.32
$\beta = 50$	0.2591	0.2135	0.1746	0.1419	0.1148
rate		0.28	0.29	0.30	0.31
$\beta = 100$	0.3378	0.3151	0.2606	0.2141	0.1748
rate		0.26	0.28	0.29	0.29
$\beta = 200$	0.5334	0.4517	0.3791	0.3156	0.2608
rate		0.24	0.25	0.26	0.28
$\beta = 400$	0.7285	0.6266	0.5345	0.4521	0.3792
rate		0.22	0.23	0.24	0.25

Table 8: Error analysis of $\frac{\|\phi_{23}(y,z) - \phi_{ho}(y,z)\|_{L^\infty}}{\|\phi_{23}(y,z)\|_{L^\infty}}$ for dimension reduction from 3D to 1D.

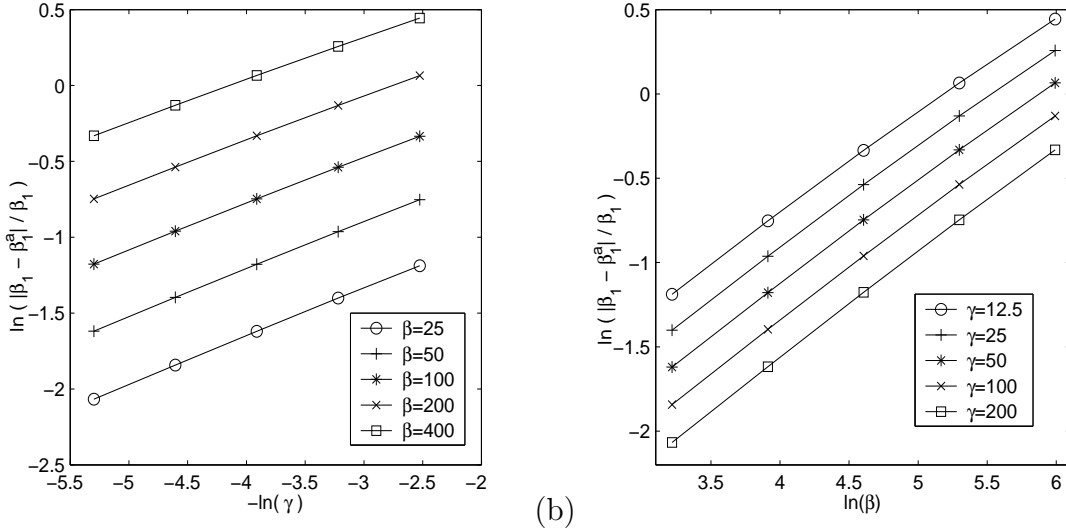


Figure 7: Convergence rate of $\frac{|\beta_1 - \beta_1^a|}{\beta_1}$ for dimension reduction from 3D to 1D: (a) With respect to $\gamma = \gamma_y = \gamma_z$; (b) with respect to β .

and $\beta = 10$ [4, 8]; and $\psi^{3D}(x, y, z, t)$ be the numerical solution of the 3D GPE (1.3) with $\gamma_x = \gamma_y = 1$ and $\beta = 10$ and the initial data $\psi(x, y, z, 0) = \psi_0^{3D}(x, y, z)$ chosen as

$$\psi_0^{3D}(x, y, z) = \frac{\phi_1^{3D}(x - x_0, y, z)\phi_1^{3D}(x + x_0, y, z)}{\|\phi_1^{3D}(x - x_0, y, z)\phi_1^{3D}(x + x_0, y, z)\|_{L^2}}, \quad (x, y, z) \in \mathbb{R}^3,$$

where $x_0 > 0$ is a constant. This 3D dynamics of BEC corresponds to the interaction of two vortex lines in 3D. Formally, when $\gamma_z \gg 1$ [4, 8, 5],

$$\phi_3(z) = \left(\int_{\mathbb{R}^2} |\psi_0^{3D}(x, y, z)|^2 dx dy \right)^{1/2} \approx \frac{(2\gamma_z)^{1/4}}{\pi^{1/4}} e^{-\gamma_z z^2} \neq \phi_{ho}(z).$$

Similarly, let $\phi_1^{2D}(x, y, z)$ be the central vortex state with winding number $m = 1$ of the 2D GPE (3.2) with $\gamma_x = \gamma_y = 1$ and $\beta_2 = \beta\sqrt{\frac{\gamma_z}{2\pi}}$ [4, 8]; and $\psi^{2D}(x, y, t)$ be the numerical solution of the 2D GPE (3.2) with $\gamma_x = \gamma_y = 1$ and $\beta_2 = \beta\sqrt{\frac{\gamma_z}{2\pi}}$ and the initial data $\psi(x, y, 0) = \psi_0^{2D}(x, y)$ chosen as

$$\psi_0^{2D}(x, y) = \frac{\phi_1^{2D}(x - x_0, y)\phi_1^{2D}(x + x_0, y)}{\|\phi_1^{2D}(x - x_0, y)\phi_1^{2D}(x + x_0, y)\|_{L^2}}, \quad (x, y) \in \mathbb{R}^2.$$

Again, this 2D dynamics of BEC corresponds to the interaction of two vortices in 2D. Let $\mathbf{x}_{2D}(t) = (x(t), y(t))^T$ be the location at time t of center of the vortex initially located at $(x_0, 0)$ in the 2D dynamics, and $\mathbf{x}_{3D}(t) = (x(t), y(t))^T$ be the location in the xy -plane at time t of center of the vortex initially located at $(x_0, 0, 0)$ in the 3D dynamics, i.e. center of the vortex from the wave function $\psi^{3D}(x, y, 0, t)$. Figure 8 shows the trajectory of $\mathbf{x}_{2D}(t)$ and $\mathbf{x}_{3D}(t)$ with $x_0 = 1$ for different γ_z .

From Fig. 8, for fixed γ_z , the trajectories of the vortex centers in 2D and 3D dynamics agree qualitatively (cf. Fig. 8). But for fixed $\beta = O(1)$, when $\gamma_z \rightarrow \infty$, the larger is γ_z , the larger is the error. This is because for larger γ_z the condensate becomes flat and thus the vortex line dynamics in 3D bent more frequently which causes the oscillatory nature in the trajectory.

For dimension reduction of the GPE with general initial data, we refer to [6, 10, 30].

4 Conclusion

Dimension reduction of the three-dimensional (3D) Gross-Pitaevskii equation (GPE) for Bose-Einstein condensation under different limiting parameter regimes was studied asymptotically and numerically. For ground state of the 3D GPE, we found the convergence rate of the reduction and provided the approximate energy and chemical potential in both disk-shaped condensation and cigar-shaped condensation. Our extensive numerical results confirmed the reduction and the convergence rate. In addition, we identified the parameter regimes in which the reduction is invalid. For dynamics of the 3D GPE, our numerical results confirmed the reduction and provided convergence rates in certain limiting parameter regime.

Appendix: Energy and chemical potential approximations for the ground states

The 3D time-independent GPE (1.5), 2D GPE (2.9) and 1D GPE (2.24) can be written in a unified way [17, 5, 7]

$$\mu \phi(\mathbf{x}) = -\frac{1}{2}\nabla^2 \phi(\mathbf{x}) + V_d(\mathbf{x})\phi(\mathbf{x}) + \beta_d|\phi(\mathbf{x})|^2\phi(\mathbf{x}), \quad \mathbf{x} \in \mathbb{R}^d, \quad (\text{A.1})$$

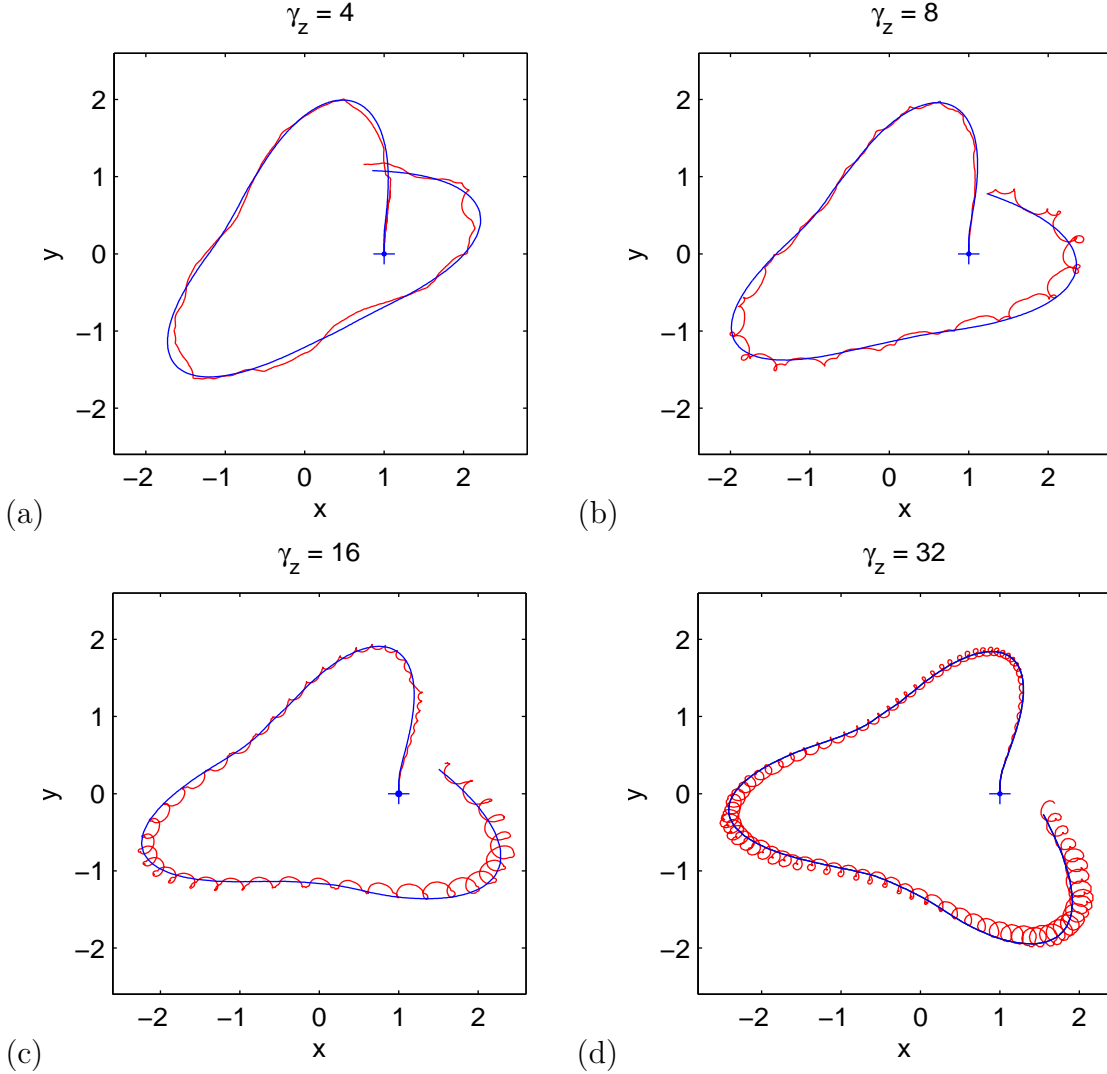


Figure 8: Trajectory of the vortex centers in 2D and 3D dynamics. Blue line (or flat curve): $\mathbf{x}_{2D}(t)$; and red line (or oscillatory curve): $\mathbf{x}_{3D}(t)$.

under the normalization condition

$$\|\phi\|^2 := \int_{\mathbb{R}^d} |\phi(\mathbf{x})|^2 d\mathbf{x} = 1; \quad (\text{A.2})$$

where $\beta_3 = \beta$, $\beta_2 = \beta_2^a$, $\beta_1 = \beta_1^a$ and $V_3(\mathbf{x}) = V(\mathbf{x})$. The energy functional is defined as

$$E(\phi) = \int_{\mathbb{R}^3} \left[\frac{1}{2} |\nabla \phi(\mathbf{x})|^2 + V(\mathbf{x}) |\phi(\mathbf{x})|^2 + \frac{\beta}{2} |\phi(\mathbf{x})|^4 \right] d\mathbf{x}. \quad (\text{A.3})$$

A1. Thomas-Fermi (TF) approximate energy and chemical potential.

When $\beta_d \gg 1$, and $\gamma_y = O(1)$ with $d = 2$ or $\gamma_y = O(1)$ and $\gamma_z = O(1)$ with $d = 3$ in (A.1), we can ignore the kinetic term and derive the TF approximation:

$$\mu_g^{\text{TF}} \phi_g^{\text{TF}}(\mathbf{x}) = V_d(\mathbf{x}) \phi_g^{\text{TF}}(\mathbf{x}) + \beta_d |\phi_g^{\text{TF}}(\mathbf{x})|^2 \phi_g^{\text{TF}}(\mathbf{x}), \quad \mathbf{x} \in \mathbb{R}^d. \quad (\text{A.4})$$

Solving (A.4), we obtain the TF approximation for the ground state:

$$\phi_g^{\text{TF}}(\mathbf{x}) = \begin{cases} \sqrt{(\mu_g^{\text{TF}} - V_d(\mathbf{x})) / \beta_d}, & V_d(\mathbf{x}) \leq \mu_g^{\text{TF}}, \\ 0, & \text{otherwise.} \end{cases} \quad (\text{A.5})$$

Plugging (A.5) into (A.2) with $\phi = \phi_g^{\text{TF}}$, we obtain [5, 7]

$$\mu_g^{\text{TF}} = \frac{1}{2} \begin{cases} \left(\frac{3\beta_1}{2}\right)^{2/3}, & d = 1, \\ \left(\frac{8\beta_2\gamma_y}{2\pi}\right)^{1/2}, & d = 2, \\ \left(\frac{15\beta\gamma_y\gamma_z}{4\pi}\right)^{2/5}, & d = 3. \end{cases} \quad (\text{A.6})$$

Since $\phi_g^{\text{TF}}(\mathbf{x})$ is not differentiable at $V_d(\mathbf{x}) = \mu_g^{\text{TF}}$, as observed in [7, 5, 8], $E(\phi_g^{\text{TF}}) = \infty$, thus one cannot use the definition (A.3) to define the energy of the TF approximation (A.5). Therefore, noticing (1.6) and (1.8), as observed in [8], here we used the way to calculate it:

$$E_g^{\text{TF}} \approx E_g = E(\phi_g) = \mu(\phi_g) - E_{\text{int}}(\phi_g) \approx \mu_g^{\text{TF}} - E_{\text{int}}(\phi_g^{\text{TF}}) = \frac{d+2}{d+4} \mu_g^{\text{TF}}. \quad (\text{A.7})$$

A2. First-order approximate energy and chemical potential.

When $\gamma_y = 1$ with $d = 2$ or $\gamma_y = \gamma_z = 1$ with $d = 3$ in (1.5), the ground state of the nonlinear eigenvalue problem (A.1) is symmetric, i.e. $\phi_g(\mathbf{x}) = \phi(r)$ with $r = |\mathbf{x}|$, and satisfies:

$$-\frac{1}{2r^{d-1}} \frac{d}{dr} \left(r^{d-1} \frac{d\phi(r)}{dr} \right) + (V_d(r) - \mu) \phi(r) + \beta_d \phi^3(r) = 0, \quad 0 < r < \infty, \quad (\text{A.8})$$

where $V_d(r) = r^2/2$. Following the method used in [29] for $d = 3$, we choose $R = \sqrt{2\mu_g^{\text{TF}}}$ such that $V_d(R) = \frac{R^2}{2} = \mu_g^{\text{TF}}$. When $|r - R| \ll R$, we have

$$V_d(r) - \mu \approx V_d(r) - \mu_g^{\text{TF}} = \frac{r^2}{2} - \frac{R^2}{2} = (r - R) \frac{r + R}{2} \approx (r - R)R. \quad (\text{A.9})$$

Noticing (A.9) and dropping the first order term $\frac{d-1}{2r} \frac{d\phi(r)}{dr}$ in (A.8), we obtain

$$-\frac{1}{2} \frac{d^2\phi(r)}{dr^2} + (r - R)R\phi(r) + \beta_d \phi^3(r) = 0, \quad 0 < r < \infty. \quad (\text{A.10})$$

Introducing a change of variables, $s = (r - R)/l$ and $\phi(r) = \alpha\tilde{\phi}(s)$ with $2Rl^3 = 1$ and $2\beta_d\alpha^2l^2 = 1$, we can reduce (A.10) to

$$\tilde{\phi}''(s) - (s + \tilde{\phi}^2(s))\tilde{\phi}(s) = 0, \quad -\infty < s < \infty. \quad (\text{A.11})$$

For the solution of (A.11), as $s \rightarrow +\infty$, $\tilde{\phi} \rightarrow 0$, dropping $\tilde{\phi}^3$ term in (A.11), we have

$$\tilde{\phi}''(s) - s\tilde{\phi}(s) = 0. \quad (\text{A.12})$$

Thus we have the asymptotics for the solution [29]:

$$\tilde{\phi}(s \rightarrow +\infty) \sim \frac{A}{2s^{1/4}} e^{-\frac{2}{3}s^{2/3}}, \quad A \approx 0.794. \quad (\text{A.13})$$

On the other hand, as $s \rightarrow -\infty$, dropping $\tilde{\phi}''(s)$ in (A.11), we have

$$s + \tilde{\phi}^2(s) = 0. \quad (\text{A.14})$$

Thus we get

$$\tilde{\phi}(s \rightarrow -\infty) \sim \sqrt{-s}. \quad (\text{A.15})$$

Choosing ε such that $l \ll \varepsilon \ll R$, using $\phi_g \approx \phi_g^{\text{TF}}$ for $r \in [0, R - \varepsilon]$ and $\phi_g \approx \alpha \tilde{\phi}((r - R)/l)$ for $r \in [R - \varepsilon, \infty)$, plugging (A.5), (A.15) and (A.6) with $\gamma_y = \gamma_z = 1$ into (1.8), we get the approximate kinetic energy of the ground state

$$\begin{aligned} E_{\text{kin}}(\phi_g) &= \frac{1}{2} \int_{\mathbb{R}^d} |\nabla \phi_g|^2 d\mathbf{x} = \frac{C_d}{2} \int_0^\infty (\phi'_g(r))^2 r^{d-1} dr \\ &= \frac{C_d}{2} \left[\int_0^{R-\varepsilon} (\phi'_g(r))^2 r^{d-1} dr + \int_{R-\varepsilon}^\infty (\phi'_g(r))^2 r^{d-1} dr \right] \\ &\approx \frac{C_d}{2} \left[\int_0^{R-\varepsilon} \left(\frac{d\phi_g^{\text{TF}}(r)}{dr} \right)^2 r^{d-1} dr + \int_{-\varepsilon/l}^\infty \frac{\alpha^2}{l^2} |\tilde{\phi}'(s)|^2 (ls + R)^{d-1} l ds \right] \\ &= \frac{C_d}{2} \left[\frac{1}{2\beta_d} \int_0^{R-\varepsilon} \frac{r^{d+1}}{2\mu_g^{\text{TF}} - r^2} dr + \frac{\alpha^2 R^{d-1}}{l} \int_{-\varepsilon/l}^\infty |\tilde{\phi}'(s)|^2 \left(1 + \frac{ls}{R}\right)^{d-1} ds \right] \\ &\approx \frac{C_d}{2} \left[\frac{1}{2\beta_d} \int_0^{R-\varepsilon} \frac{r^{d+1}}{2\mu_g^{\text{TF}} - r^2} dr + \frac{\alpha^2 R^{d-1}}{l} \int_{-\varepsilon/l}^\infty |\tilde{\phi}'(s)|^2 ds \right] \\ &\approx \frac{C_d}{2} \left[\frac{R^d}{4\beta_d} \left(\ln \frac{R}{2\varepsilon} + D_d \right) + \frac{\alpha^2 R^{d-1}}{l} \int_{-\varepsilon/l}^\infty |\tilde{\phi}'(s)|^2 \sqrt{1+s^2} d \ln(s + \sqrt{1+s^2}) \right] \\ &\approx \frac{C_d}{2} \left[\frac{R^d}{4\beta_d} \left(\ln \frac{R}{2\varepsilon} + D_d \right) + \frac{\alpha^2 R^{d-1}}{4l} \left(\ln \frac{2\varepsilon}{l} + C \right) \right] \\ &\approx \frac{C_d}{2} \left[\frac{R^d}{4\beta_d} \left(\ln \frac{R}{2\varepsilon} + D_d \right) + \frac{R^d}{4\beta_d} \left(\ln(2\varepsilon(2R)^{1/3}) + C \right) \right] \\ &= \frac{C_d R^d}{8\beta_d} \left[\ln(2^{1/3} R^{4/3}) + D_d + C \right] = \frac{\tilde{C}_d}{\beta_d^{2/(d+2)}} (\ln \beta_d + G_d), \quad (\text{A.16}) \end{aligned}$$

where

$$\begin{aligned} C &= -4 \int_{-\varepsilon/l}^\infty \ln(\sqrt{1+s^2} + s) \frac{d}{ds} \left[\sqrt{1+s^2} (\tilde{\phi}'(s))^2 \right] ds \\ &\approx -4 \int_{-\infty}^\infty \ln(\sqrt{1+s^2} + s) \frac{d}{ds} \left[\sqrt{1+s^2} (\tilde{\phi}'(s))^2 \right] ds \approx 0.706, \\ R &= \sqrt{2\mu_g^{\text{TF}}} = \left[\frac{((d+1)^2 - 1)\beta_d}{C_d} \right]^{1/(d+2)}, \end{aligned}$$

$$\begin{aligned}\tilde{C}_d &= \frac{C_d^{2/(d+2)}((d+1)^2 - 1)^{d/(d+2)}}{6(d+2)}, \quad d = 1, 2, 3, \\ G_d &= \ln \frac{(d+1)^2 - 1}{C_d} + \frac{d+2}{4} (\ln 2 + 3D_d + 3C),\end{aligned}$$

$$C_d = \begin{cases} 2, & d = 1 \\ 2\pi, & d = 2 \\ 4\pi, & d = 3. \end{cases} \quad D_d = \begin{cases} \ln 4 - 2, & d = 1 \\ -1, & d = 2 \\ \ln 4 - 8/3, & d = 3. \end{cases}$$

From (A.3), (A.7), (1.6), (1.8), (A.4) and (A.16), we can get the first order approximation for E_g and μ_g when $\beta_d \gg 1$:

$$\begin{aligned}E_g &\approx E_g^{\text{TF}} + E_{\text{kin}}(\phi_g) \approx \frac{d+2}{2(d+4)} \left[\frac{((d+1)^2 - 1)\beta_d}{C_d} \right]^{2/(d+2)} + \frac{\tilde{C}_d}{\beta_d^{2/(d+2)}} (\ln \beta_d + G_d) \\ &= \frac{d+2}{2(d+4)} \left[\frac{((d+1)^2 - 1)\beta_d}{C_d} \right]^{2/(d+2)} + O\left(\frac{\ln \beta_d}{\beta_d^{2/(d+2)}}\right),\end{aligned}\tag{A.17}$$

$$\begin{aligned}\mu_g &\approx \mu_g^{\text{TF}} + E_{\text{kin}}(\phi_g) \approx \frac{1}{2} \left[\frac{((d+1)^2 - 1)\beta_d}{C_d} \right]^{2/(d+2)} + \frac{\tilde{C}_d}{\beta_d^{2/(d+2)}} (\ln \beta_d + G_d) \\ &= \frac{1}{2} \left[\frac{((d+1)^2 - 1)\beta_d}{C_d} \right]^{2/(d+2)} + O\left(\frac{\ln \beta_d}{\beta_d^{2/(d+2)}}\right).\end{aligned}\tag{A.18}$$

These asymptotic results were confirmed by the numerical results in [7].

Acknowledgment

The first two authors acknowledge support by the National University of Singapore grant No. R-146-000-083-112. P.A.M. acknowledges support from the EU-funded TMR network ‘Asymptotic Methods in kinetic Theory’, from his WITTGENSTEIN-AWARD 2000 funded by the Austrian National Science Fund FWF. W.B. also acknowledges support from the WITTGENSTEIN-AWARD of P. Markowich and the hospitality of the Wolfgang Pauli Institute in Vienna for his extended visit.

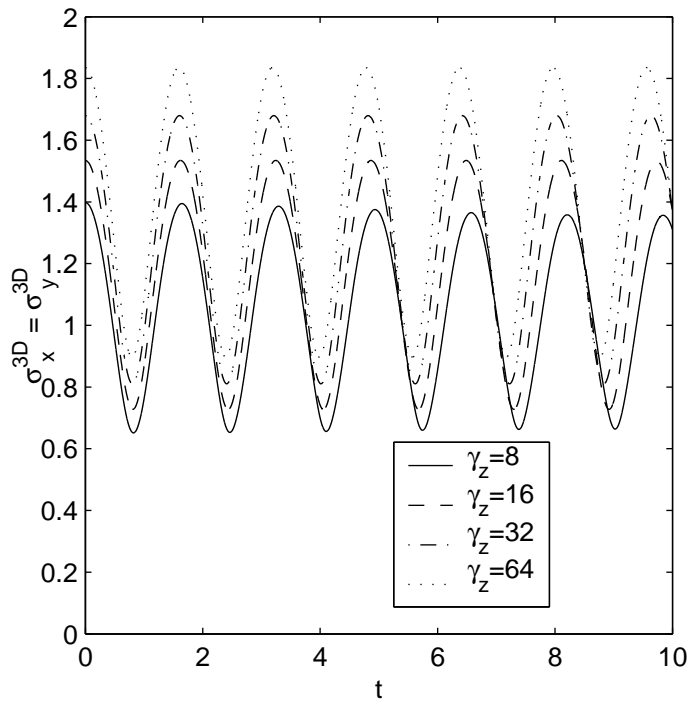
References

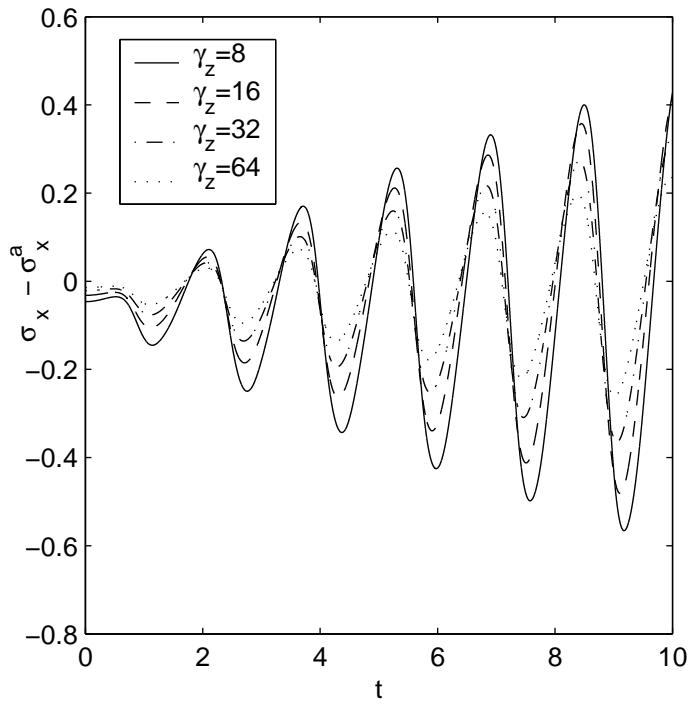
- [1] M. H. Anderson, J. R. Ensher, M. R. Matthews, C. E. Wieman and E. A. Cornell, Observation of Bose-Einstein condensation in a dilute atomic vapor, *Science*, 269 (1995), pp. 198-201.

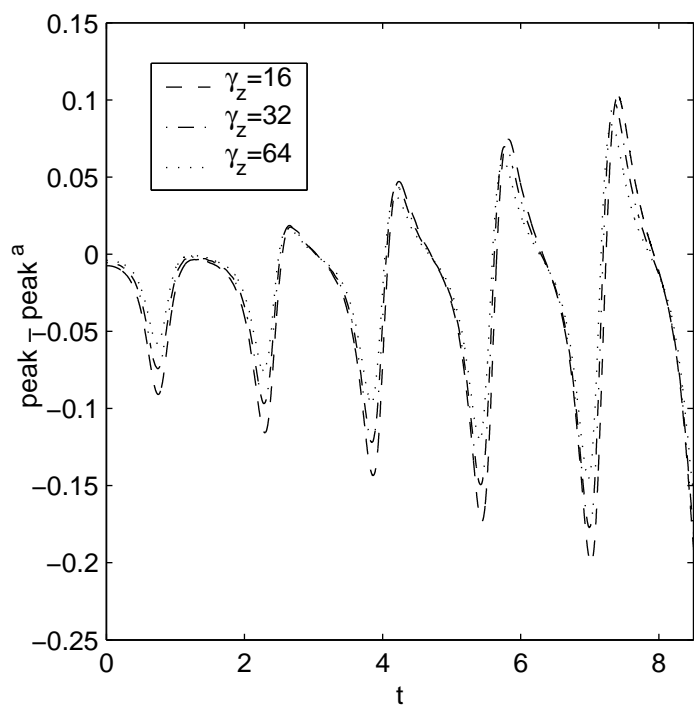
- [2] J.R. Anglin and W. Ketterle, Bose-Einstein condensation of atomic gases, *Nature*, 416 (2002), pp. 211–218.
- [3] W. Bao, Ground states and dynamics of multi-component Bose-Einstein condensates, *Multiscale Modeling and Simulation*, 2 (2004), pp. 210-236.
- [4] W. Bao and Q. Du, Computing the ground state solution of Bose-Einstein condensates by a normalized gradient flow, *SIAM J. Sci. Comp.*, 25 (2004), pp. 1674-1697.
- [5] W. Bao, D. Jaksch and P.A. Markowich, Numerical solution of the Gross-Pitaevskii equation for Bose-Einstein condensation, *J. Comput. Phys.*, 187 (2003), pp. 318-342.
- [6] W. Bao, P. A. Markowich, C. Schmeiser and R. M. Weishaupl, On the Gross-Pitaevskii equation with strongly anisotropic confinement: formal asymptotics and numerical experiments, *Math. Mod. Meth. Appl. Sci.*, 15 (2005), pp. 767-782.
- [7] W. Bao and W. Tang, Ground state solution of trapped interacting Bose-Einstein condensate by directly minimizing the energy functional, *J. Comput. Phys.*, 187(2003), pp. 230-254.
- [8] W. Bao and Y. Zhang, Dynamics of the ground state and central vortex states in Bose-Einstein condensation, *Math. Mod. Meth. Appl. Sci.*, 15 (2005), pp. 1863-1896.
- [9] G. Baym and C.J. Pethick, Ground-state properties of magnetically trapped Bose-condensed Rubidium gas, *Phys. Rev. Lett.*, 76 (1996), pp. 6-9.
- [10] N. Ben Abdallah, F. Mehats, C. Schmeiser and R. M. Weishäupl, The nonlinear Schrödinger equation with a strongly anisotropic harmonic potential, *SIAM J. Math. Anal.*, 37 (2005), pp. 189–199.
- [11] C. C. Bradley, C. A. Sackett, J.J. Tollett and R. G. Hulet, Evidence of Bose-Einstein condensation in an atomic gas with attractive interactions, *Phys. Rev. Lett.*, 75 (1995), pp. 1687-1690.
- [12] M.M. Cerimele, M.L. Chiofalo, F. Pistella, S. Succi and M.P. Tosi, Numerical solution of the Gross-Pitaevskii equation using an explicit finite-difference scheme: An application to trapped Bose-Einstein condensates, *Phys. Rev. E*, 62 (2000), pp. 1382-1389.
- [13] M.L. Chiofalo, S. Succi and M.P. Tosi, Ground state of trapped interacting Bose-Einstein condensates by an explicit imaginary-time algorithm, *Phys. Rev. E*, 62 (2000), pp. 7438-7444.

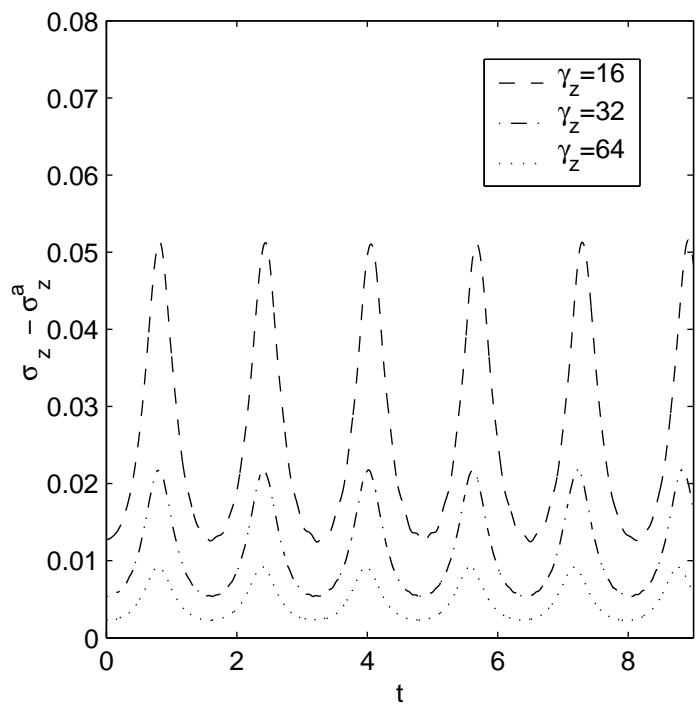
- [14] E. Cornell, Very cold indeed: The nanokelvin physics of Bose-Einstein condensation, *J. Res. Natl. Inst. Stan.*, 101 (1996), pp. 419–434.
- [15] F. Dalfovo, S. Giorgini, L.P. Pitaevskii and S. Stringari, Theory of Bose-Einstein condensation in trapped gases, *Rev. Mod. Phys.*, 71 (1999), pp. 463-512.
- [16] K. B. Davis, M. -O. Mewes, M. R. Andrews, N. J. van Druten, D. S. Durfee, D. M. Kurn and W. Ketterle, Bose-Einstein condensation in a gas of sodium atoms, *Phys. Rev. Lett.*, 75 (1995), pp. 3969-3973.
- [17] V. Dunjko, V. Lorent and M. Olshanii, Bosons in cigar-shaped traps: Thomas-Fermi Tonks-Girardeau regime, and in between, *Phys. Rev. Lett.*, 86 (2001), pp. 5413-5416.
- [18] Yunyi Ge, Dimension Reduction in Bose-Einstein Condensates, Msc. Thesis, Department of Computational Science, National University of Singapore, 2004.
- [19] E.P. Gross, Structure of a quantized vortex in boson systems, *Nuovo. Cimento.*, 20 (1961), pp. 454-477.
- [20] D. S. Hall, M. R. Matthews, J. R. Ensher, C. E. Wieman and E. A. Cornell, Dynamics of component separation in a binary mixture of Bose-Einstein condensates, *Phys. Rev. Lett.*, 81 (1998), pp. 1539-1542.
- [21] A.D. Jackson, G.M. Kavoulakis and C.J. Pethick, Solitary waves in clouds of Bose-Einstein condensed atoms, *Phys. Rev. A* 58, 2417 (1998).
- [22] L. Landau and E. Lifschitz, *Quantum Mechanics: non-relativistic theory*, Pergamon Press, New York, 1977.
- [23] P. Leboeuf and N. Pavloff, Bose-Einstein beams: coherent propagation through a guide, *Phys. Rev. A*, 64 (2001), pp. 033602;
- [24] E.H. Lieb and R. Seiringer, One-dimensional bosons in three-dimensional traps, *Phys. Rev. Lett.*, 91 (2003), 150401.
- [25] E.H. Lieb, R. Seiringer and J. Yngvason, Bosons in a trap: a rigorous derivation of the Gross-Pitaevskii energy functional, *Phys. Rev. A*, 61 (2000), 043602.
- [26] E.H. Lieb, R. Seiringer and J. Yngvason, One-dimensional behavior of dilute, trapped Bose gases, *Comm. Math. Phys.*, 244 (2004), pp. 347–393.
- [27] C.J. Pethick and H. Smith, *Bose-Einstein Condensation in Dilute Gases*, Cambridge University Press, 2002.
- [28] L.P. Pitaevskii, Vortex lines in a imperfect Bose gas, *Zh. Eksp. Teor. Fiz.*, 40 (1961), pp. 646-649. (*Sov. Phys. JETP*, 13 (1961), pp. 451-454).

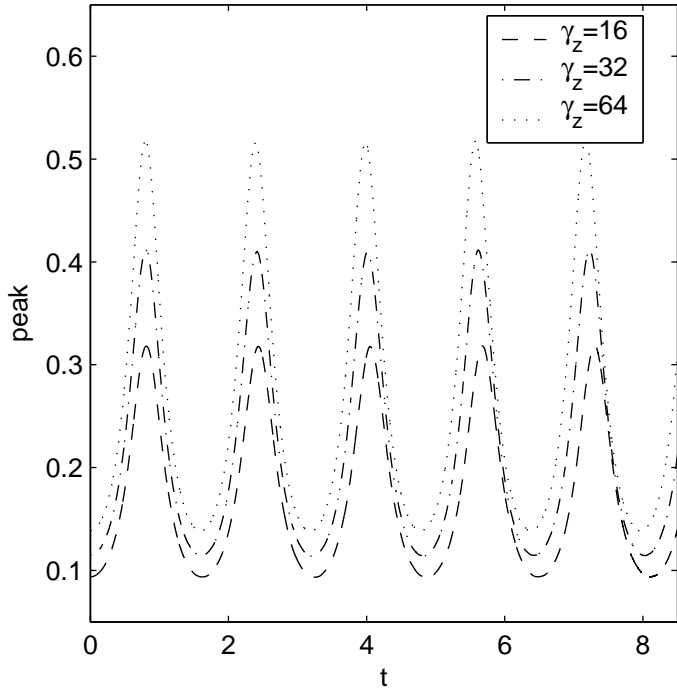
- [29] L.P. Pitaevskii and S. Stringari, Bose-Einstein condensation, Clarendon press, 2003.
- [30] L. Salasnich, A. Parola and L. Reatto, Effective Wave-Equations for the Dynamics of cigar-shaped and disc-shaped Bose condensates, Phys. Rev. A, 65 (2002), article 043614.
- [31] R. Seiringer, Ground state asymptotics of a dilute, rotating gas, J. Phys. A, 36 (2003), pp. 9755–9778.

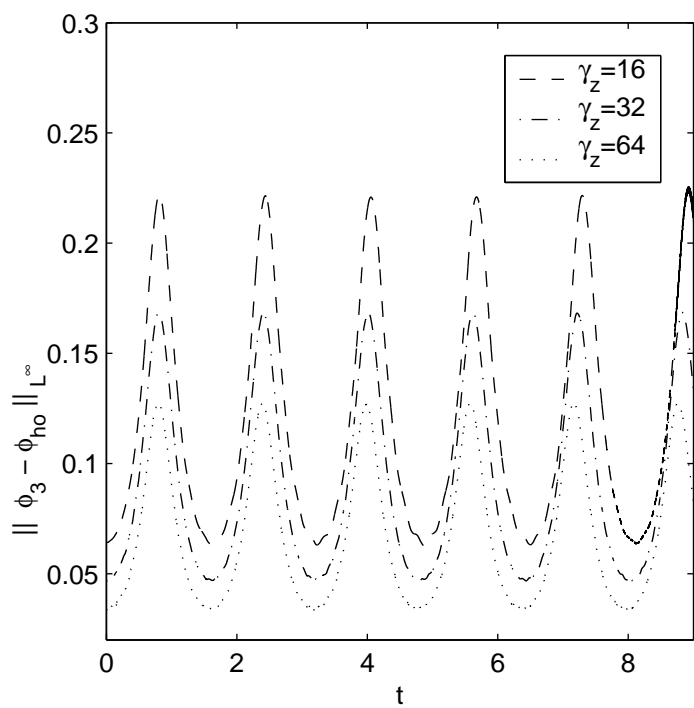


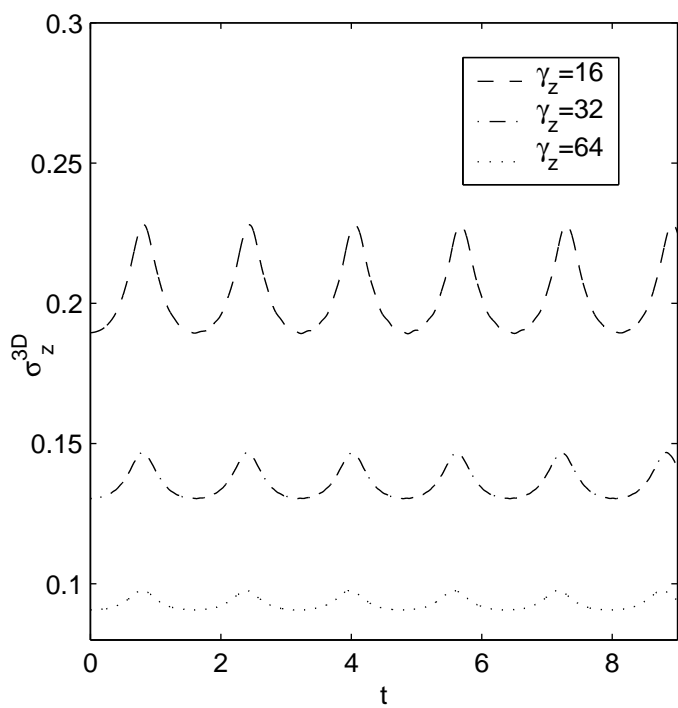


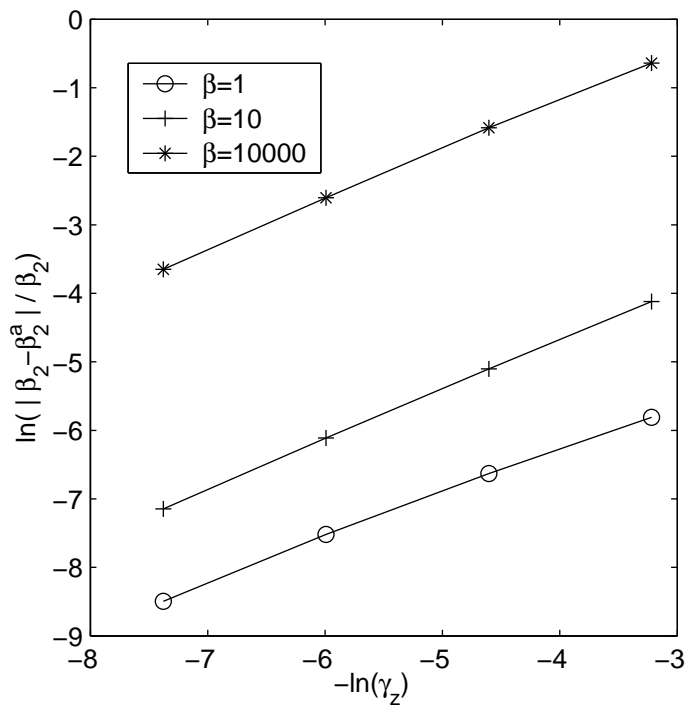


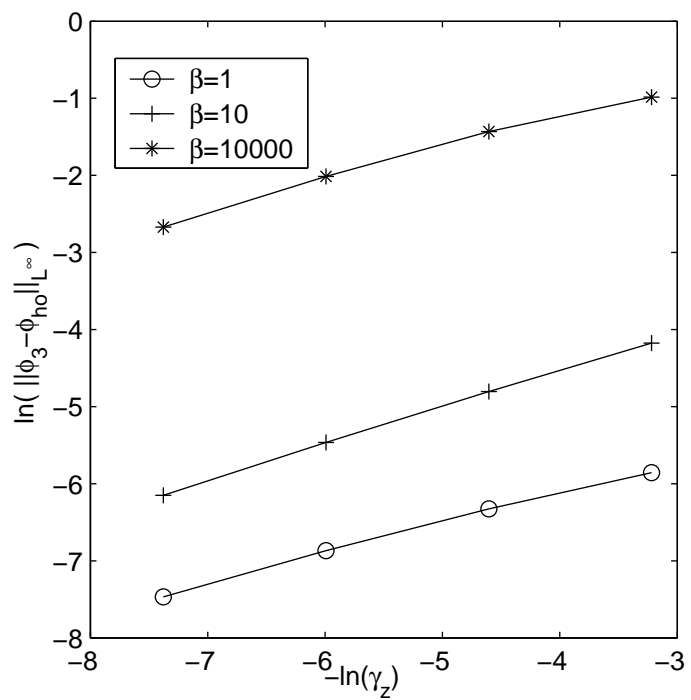


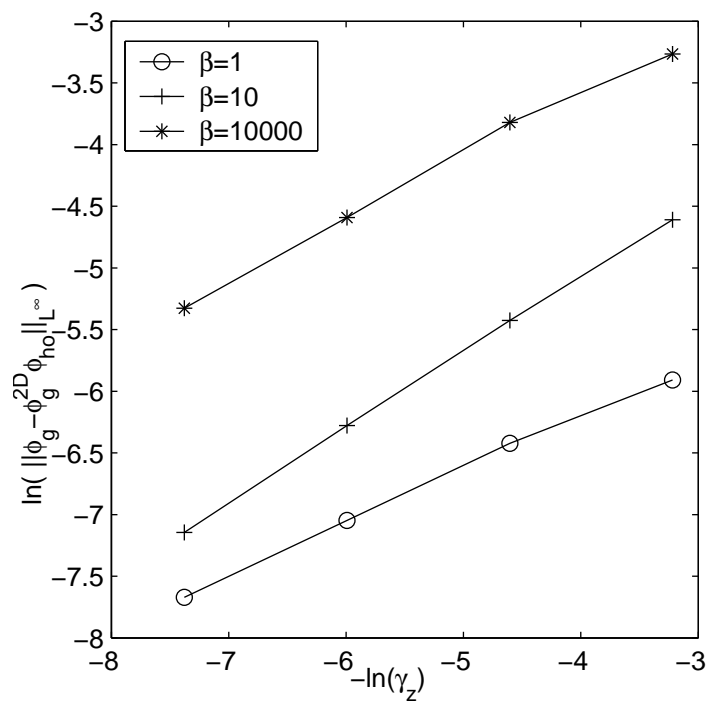


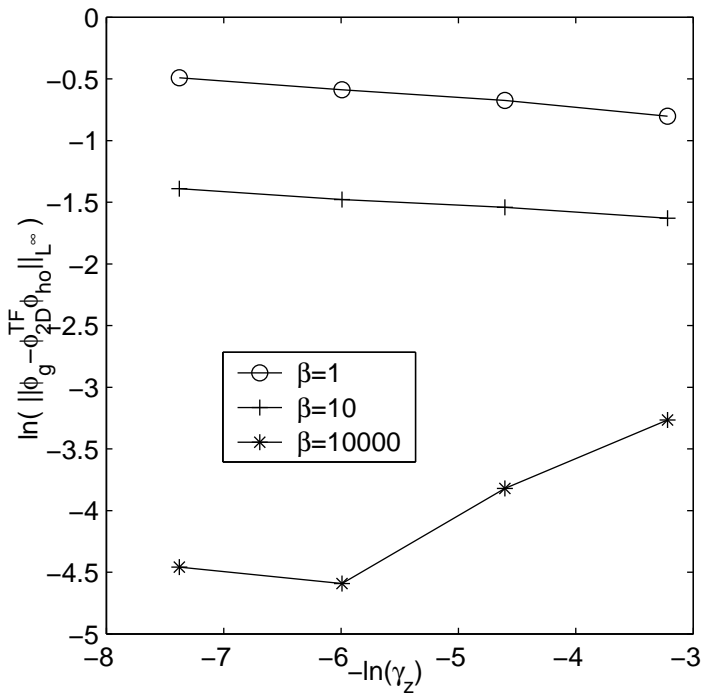


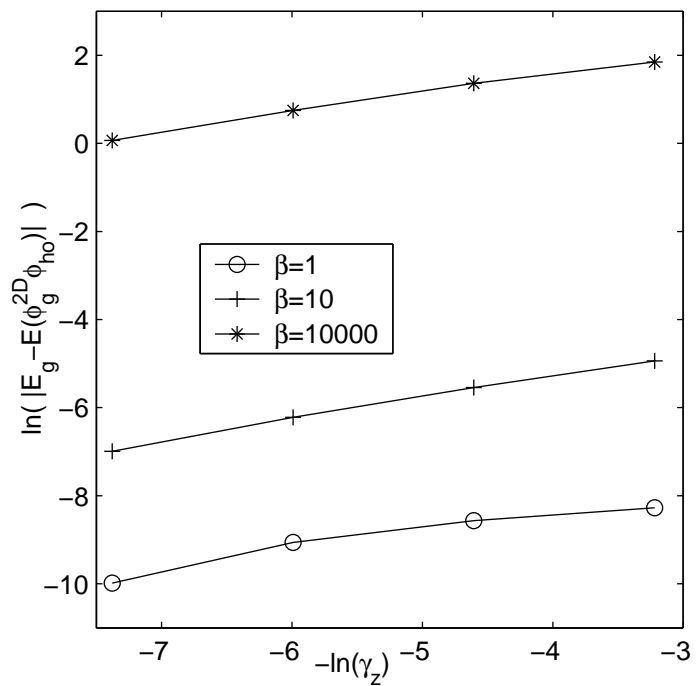


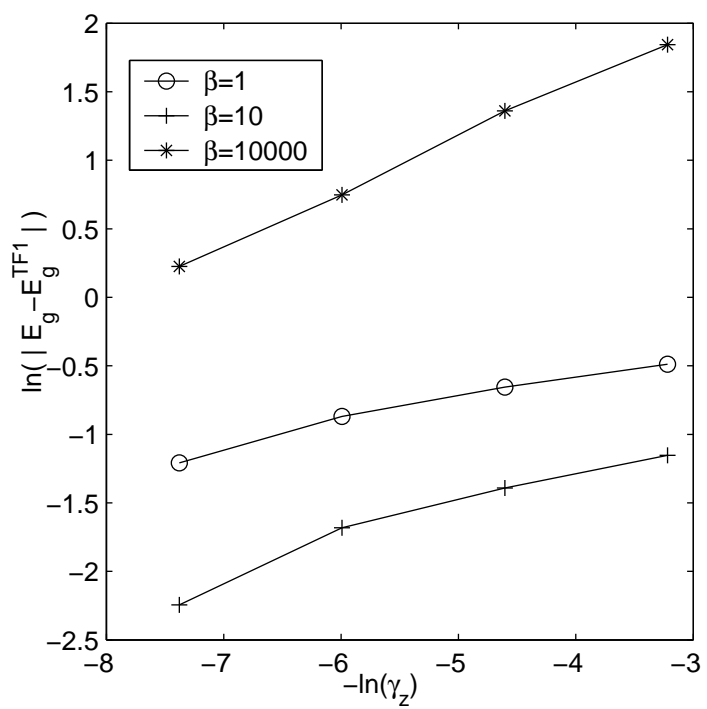


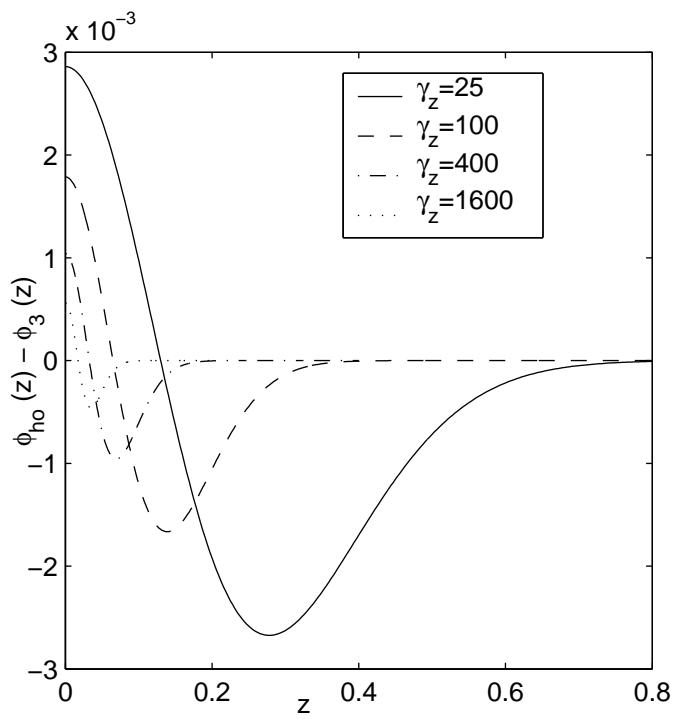


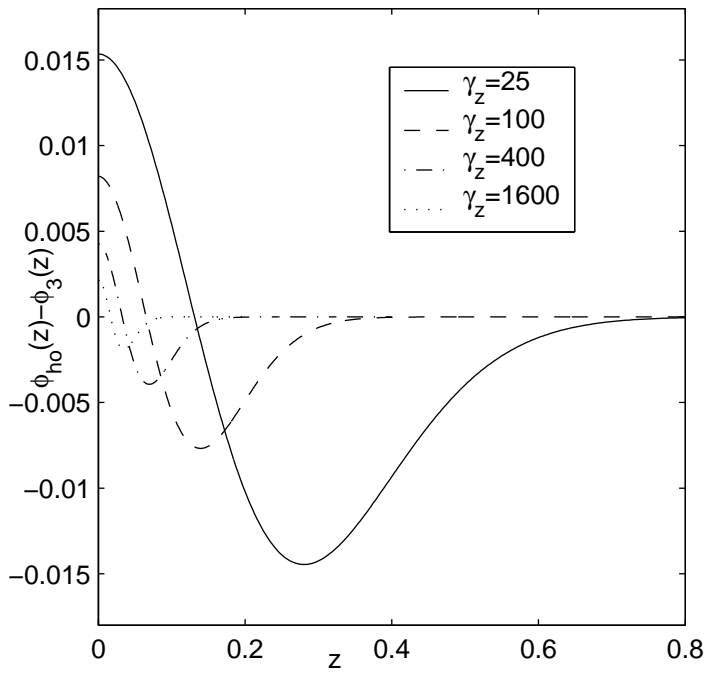


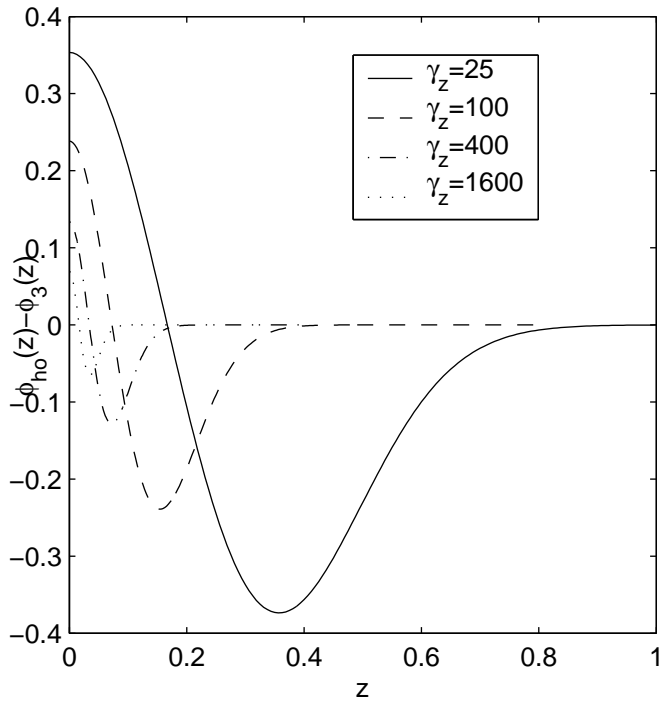


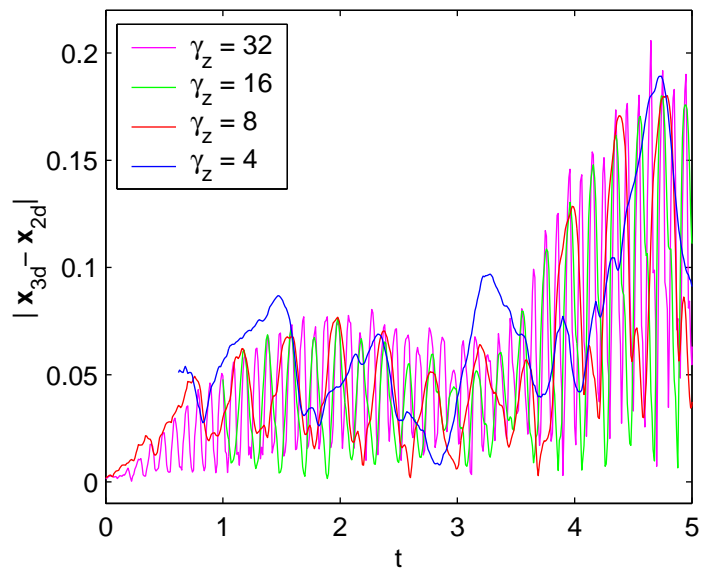


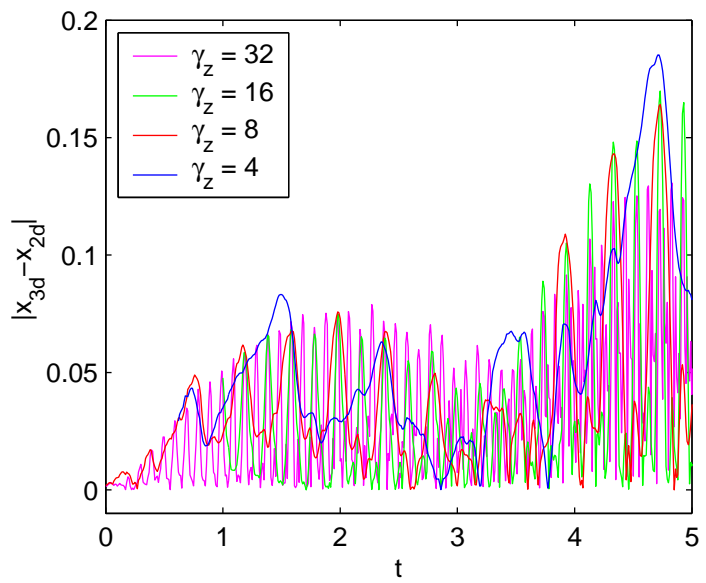


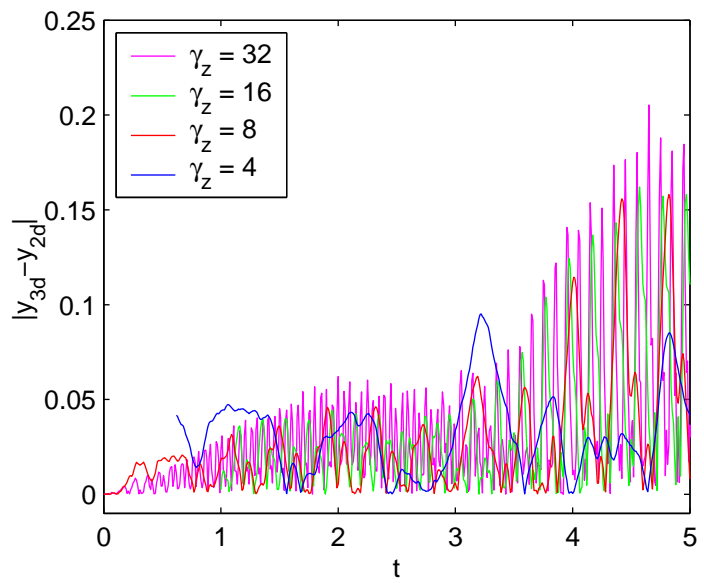


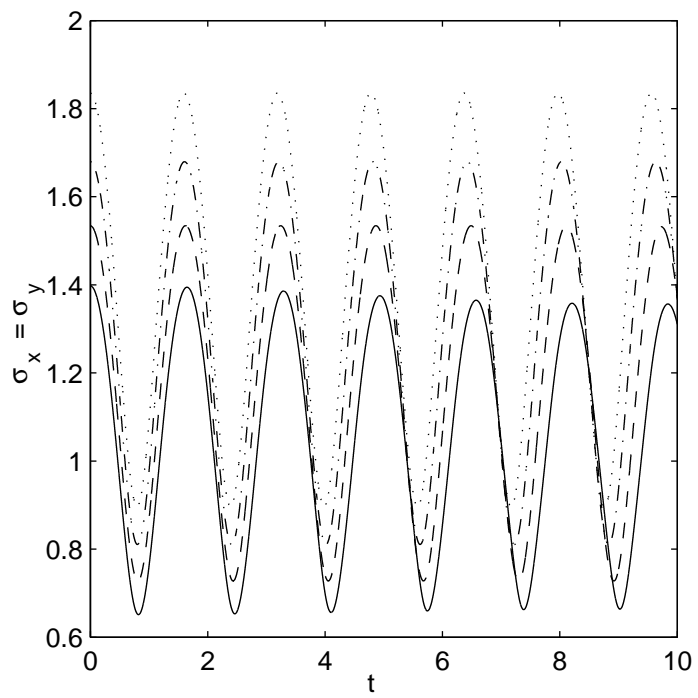


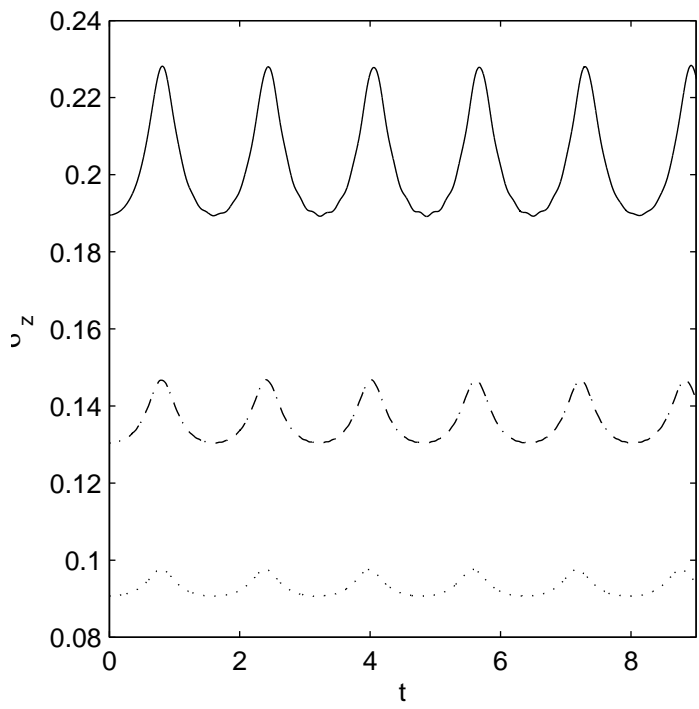


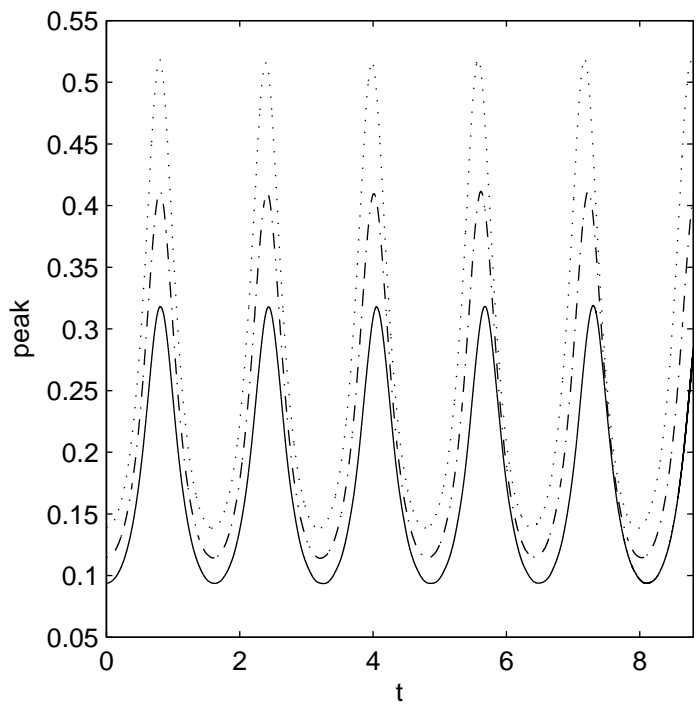




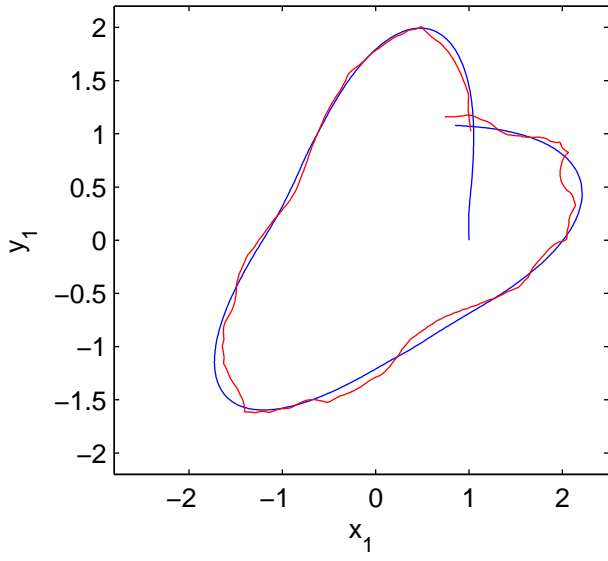




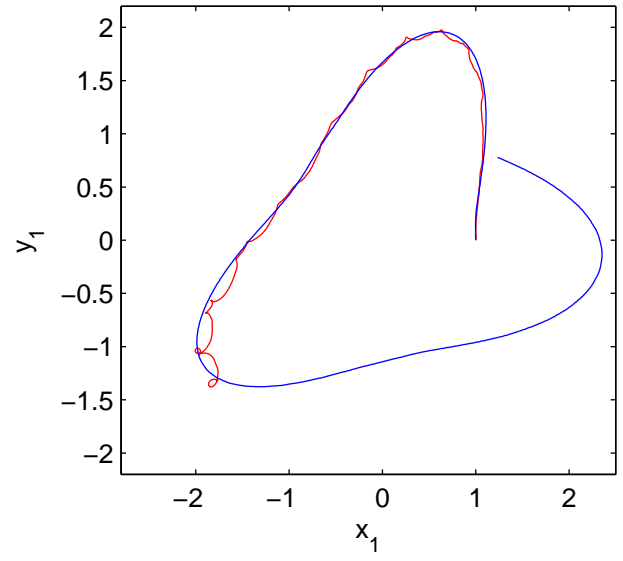




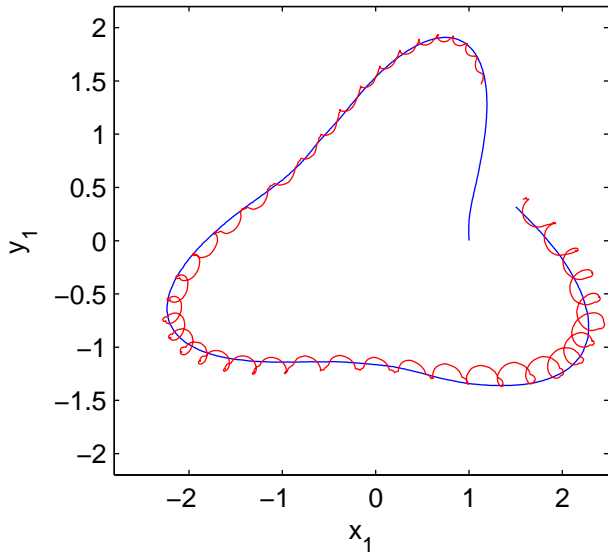
$\gamma_z = 4$



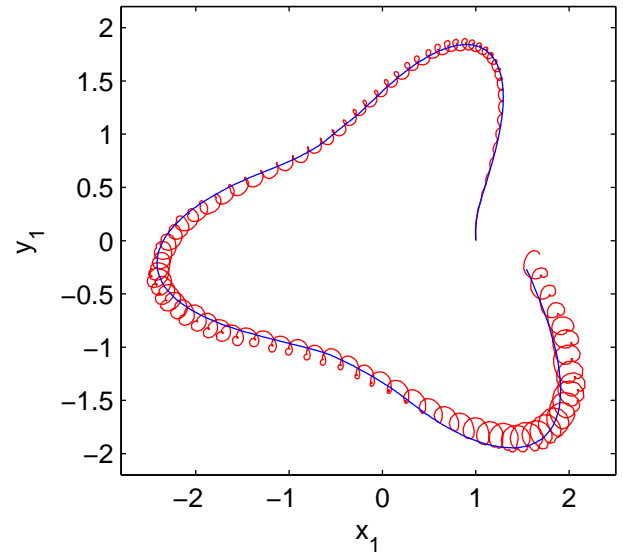
$\gamma_z = 8$



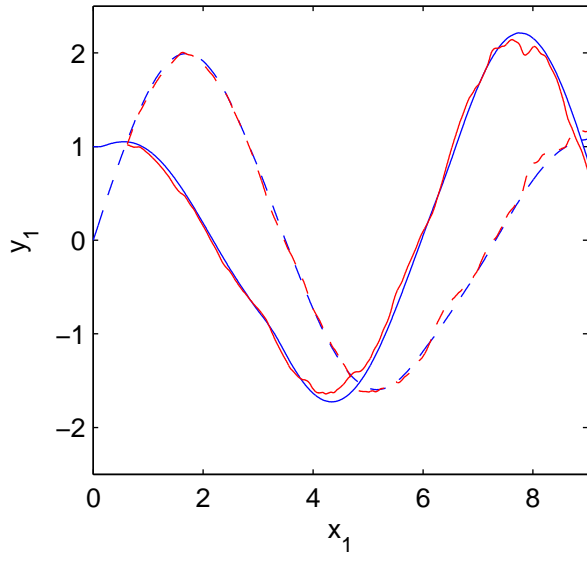
$\gamma_z = 16$



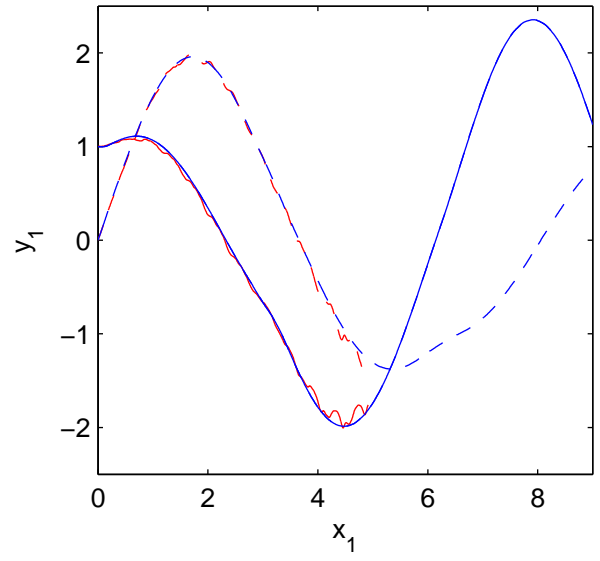
$\gamma_z = 32$



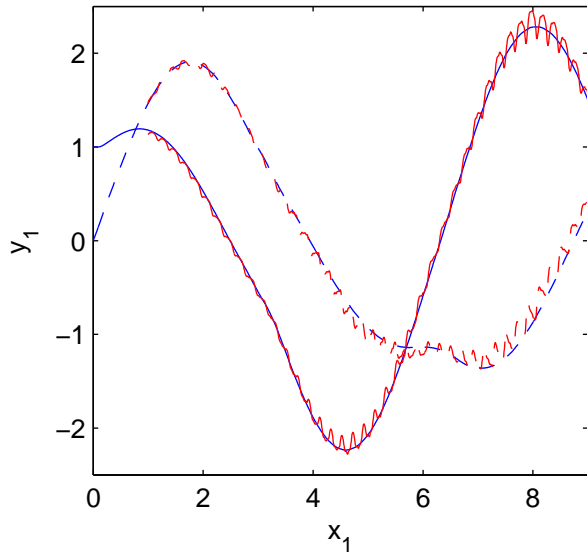
$\gamma_z = 4$



$\gamma_z = 8$



$\gamma_z = 16$



$\gamma_z = 32$

